UNBALANCE RESPONSE OF A TEST ROTOR SUPPORTED ON SQUEEZE FILM DAMPERS

by

Luis San Andrés
Daniel Lubell

April 1996

TRC-SFD-2-96

Texas A&M University
Mechanical Engineering Department

Unbalance Response of a Test Rotor Supported on Squeeze Film Dampers

by

Luis San Andres
Associate Professor
Dan Lubell
Research Assistant

A Research Progress Report
to the
Turbomachinery Research Consortium

Subject: Squeeze Film Dampers

May 1996

TRC Project:
Experimental Study of the Response of Squeeze Film Damper Supported Rotors.
Principal Investigator: Dr. Luis San Andres, Associate Professor

Unbalance Response of a Test Rotor Supported on Squeeze Film Dampers

Luis San Andres
Associate Professor
Daniel Lubell
Graduate Research Assistant
May 1996

Executive Summary

Progress in the construction, operation and testing of an apparatus for measurement of the unbalance response of a rotor-bearing system supported on squeeze film dampers (SFDs) is reported. The test rig consists of a massive three-disk rotor supported on high precision ball bearings. The bearing supports can hold conventional SFDs or integral SFDs. The conventional SFDs have a cylindrical journal supported by four elastic bar structures, while the integral SFDs have four squeeze film pads with compact S-shaped journal structural supports. The test rig is fully instrumented to perform measurements of rotor displacement at three locations along the rotor and dynamic pressures at the dampers. A data acquisition system is dedicated to perform the measurements and present system responses as bode plots, orbital graphs and discrete fast Fourier transforms. Identification of the test rig operating parameters, system natural frequencies and damping coefficients are thoroughly discussed. Experimental results demonstrate the operation of the test rig with and without the dampers operating and highlight the benefits of a squeeze film damper in dissipating undesirable vibrational energy. Rotor synchronous responses to disk imbalances show the system to be well damped with amplification factors between 1.8 and 2.0. The rotor amplitudes of motion are proportional to the imbalance displacements. Identification of the system damping coefficient shows this to be much greater than the one predicted from conventional squeeze film damper models. Further tests are planned to measure the rotor-bearing synchronous response to couple unbalances and for SFD journal off-centered conditions.

The research program is a joint effort funded by the National Science Foundation (NSF) and the Turbomachinery Research Consortium (TRC).

Table of Contents

Nomenclature

C	SFD radial clearance [m]
C_*	SFD nominal clearance [m]
C_{crit}	$2\sqrt{K_{eq} / M_{eq}}$, Critical damping coefficient for first mode [N-sec/m]
C_V, C_H	System damping coefficients for vertical and horizontal motions [N-sec/m]
C_{SFD}	SFD theoretical direct damping coefficient [N-sec/m], equation (3).
C_L	$g^3/12\mu L$, end seal coefficient [$m^2sec^{-1}Pa^{-1}$].
D	SFD diameter [m]
e	amplitude of rotor motion [m]
f_{Vn}, f_{Hn}	First natural frequencies for vertical and horizontal motions [Hz]
g	end seal gap [m]
h	squeeze film thickness [m].
L	SFD length [m]
m	unbalance mass [kg]
M_{eq}	equivalent rotor mass for first mode [kg]
k_s	SFD lateral stiffness [N/m]
K_{Veq}, K_{Heq}	System equivalent stiffness coefficients for vertical and horizontal motions [N/m]
P	squeeze film pressure [Pa]
P_e, P_a	exit and ambient pressures
Q	Amplification factor at first critical speed
r	radius for location of unbalance mass [m].

u	$= m^*r/M$, unbalance displacement [m].
t	time [sec].
μ	fluid viscosity [Pa-sec]
θ,z	circumferential and axial coordinates.
ξ	$= C_V/C_{crit}$ or $C_H/C_{crit} = 1/2Q$, system damping ratio.
ε	$= e/C_*$, dimensionless SFD journal center displacement.

Introduction

Squeeze film dampers (SFDs) provide viscous damping dissipation to rotating structures, allowing for reduction in rotor-bearing lateral vibration amplitudes and providing safe isolation to other structural components. SFDs have been used primarily in aircraft jet engines where rolling element bearings provide little damping to the rotor-bearing system, and in high performance compressors as retrofit elements in series with tilting pad bearings to soften bearing supports, reduce critical speeds, and allow for an extra margin of system stability.

Widely varying test results in research and practice have demonstrated that the design of SFDs is based on overly simplified analytical models which either fail to incorporate or simply neglect distinct structural and fluid-related features which greatly affect the dynamic force response of SFDs. The lack of adequate understanding of the mechanics of squeeze film flows stems from the near absence of fundamental experimental evidence and sound rationale that directly address the issues and problems of interest.

Rotordynamic analyses regard SFDs as non-linear mechanical elements providing film forces ranging from low to unlimited depending on the instantaneous journal position and velocity within the clearance circle (Vance, 1988). Analytical and computer-based predictions of the dynamic response of rotor-bearing systems supported on SFDs show a rich non-linear behavior with multiple valued responses, jump phenomena and even zones evidencing chaotic responses. The dynamic response of these rotor-bearing systems is extremely sensitive to imbalance levels which if large enough can lock-up the bearing supports and give rise to excessive vibration amplitudes at the most flexible points of the structure while passing through critical speeds.

Numerous papers of disputable merit present the analysis and design of simple geometry SFDs based on solutions to the classical Reynolds equation of hydrodynamic lubrication. The most popular being the short length SFD with open ends. The squeeze film action generates hydrodynamic pressures (and damping forces) at the film locations where the instantaneous gap is decreasing. On the other hand, the theoretical analysis predicts suction pressures on the regions where the film thickness is locally increasing. In these zones, the model simply assumes the lubricant to cavitate, i.e. to undergo an *instantaneous* phase change since an ideal fluid is unable to sustain tension. The theoretical model does not account for the physical aspects of bubble dynamics which must include at least local mass conservation.

The models, as given by Mohan and Hahn (1974), Li and Taylor (1987) and San Andres and Vance (1988) consider the cavitation issue as governed purely by the kinematics of journal motion rendering a cavitation zone of 180° around the journal circumference. This assumption has given gives rise to the *infamous* **SFD π-film model**. In general, theoretical predictions of rotor responses have correlated poorly with test results since dampers in practice operate with a number of features which affect their performance. The most important factors are the level of external pressurization, type of feed mechanism and end seal restrictions, fluid inertia, and most notably air

ingestion from the gaseous environment surrounding the SFDs. There is little physical evidence and practical experience attesting to the veracity of the theoretical predictions. Theoretical works are yet to provide a sound set of results (of practical value) for the design and operation of SFDs.

Current technological advances in metal working have given rise to a novel type of squeeze film damper, namely the integral SFD. This ingenious design is made possible by a wire **E**lectrical **D**ischarge **M**achining process. Figure 1 notes distinctly the features of a conventional SFD with a squirrel cage support and an integral SFD. Squeeze film dampers derive their action from a lubricant being squeezed in the annular space between a non-rotating journal and a bearing housing. The journal typically mounted on the outer race of rolling element bearings moves (in translation or precession) due to the external forces exerted on the rotating shaft. Conventional SFDs consist of a cylindrical journal and bearing with an elastic support connecting the journal to ground and preventing its rotation. This support in the form of a squirrel cage or flexure beams needs to be soft enough to allow journal motions and to bring an effective damping action. The required low stiffness of the damper supports demands a design occupying a space two or three times longer than the journal (or ball bearing) axial length.

On the other hand, integral SFDs are compact since the damper is comprised of arcuate segmented pads attached to the damper housing via thin S-shaped structural webs. These accurately machined webs integral with the damper structure provide the desired flexibility to each of the squeeze film pads. Thus, the integral SFD requires no more axial length than the ball bearings and can also be machined as split segments. These features make the integral SFDs very attractive for retro-fitting of existing machines without major modifications. Zeidan (1995) discusses successful applications of integral SFDs in industry. This novel damper technology still lacks controlled testing and a comprehensive report of their force performance has not been done. Furthermore, current analysis of integral SFDs is just an extension of the conventional SFD model, and thus further studies are needed to overcome this shortcoming. The ultimate goal is of course to validate experimental measurements with predictions based on a sound analytical model.

Objectives of the research:

The NSF-TRC research project focuses on the analysis and measurement of the imbalance response of a test rotor supported on squeeze film dampers. The test rig is designed to house conventional dampers with a four-bar elastic centering mechanism that simulates a squirrel cage, and integral SFDs with thin S-shaped elastic supports fabricated with a wire EDM. This novel type of damper allows for a more compact design and permits rapid retrofitting in a practical situation.

Most rotor-bearing systems incorporating squeeze film dampers have soft elastic supports to render the dampers effective while traversing rigid body critical speeds. Safety considerations at the Laboratory limit the test-rotor speed to a maximum of 9,000 rpm. The test rotor, designed with cylindrical and conical mode critical speeds below this top speed, has been constructed and it

is currently in operation. A description of the test rig, operation and instrumentation is presented in the next sections. The major objectives of the research program are the following:

a) To provide relevant rotordynamic predictions and measurement of the imbalance forced response of the test rotor supported on conventional SFDs and integral SFDs.
b) To develop an experimentally validated analytical model to predict the forced dynamic performance of conventional SFDs and integral SFDs. The model should include operation of the damper with a (bubbly) air/oil mixture that arises in typical operation due to air ingestion.
c) If the test results should show significant deviations from linearity in their frequency responses, to develop a non-linear fluid-structural model more likely to reproduce the measurements.
d) To correlate the dynamic performances of the test rotor supported on both conventional SFDs and integral SFDs, to indicate the advantages and disadvantages of one mechanical element over the other, and to provide recommendations for applications in industry.

Several tasks must be performed to accomplish successfully the aforementioned objectives. These are briefly:

a) **Prediction of fundamental system parameters.** Using a commercial linear rotordynamics software, predict the first and second free-free mode natural frequencies of the test rotor, calculate the system undamped critical speeds and damped eigenvalues, and calculate the synchronous response of the rotor-damper system for imbalance masses similar to those used in the measurement test matrix. Values of the damper's structural stiffness and damping coefficients are needed and obtained from in-situ measurements using static load-displacement measurements and transfer function responses to impact excitations.
b) **Measurement of fundamental rotor-bearing system parameters.** These include independent tests for measurement of the lateral stiffness of the squirrel cage in the conventional damper, measurement of the fundamental free-free mode natural frequency of the test rotor, experimental determination of the system inherent or residual damping before the dampers are filled with lubricant, measurement of the lubricant viscosity at different temperatures, and identification of the rotor-SFD system damping coefficients at null rotational speed and as a function of the oil temperature. Correlation with calculated predictions is mandatory after each task is completed to insure proper rotordynamics modeling of the system.
c) **Measurements of the imbalance response of the test rotor**. Controlled coast-down tests of the rotor without imbalance (baseline) and imbalance masses located at the disks are to be conducted. Analysis of the synchronous responses at the locations of measurements will determine the effectiveness of the SFDs as well as the linearity of the responses.
d) **Develop a computational model for calculation of the dynamic pressure field and fluid film forces in integral SFDs**. Little is known in the open literature about the analysis and design of integral SFDs. However, inquiries with the manufacturer of these dampers indicate that computed damping coefficients are extracted from the conventional cylindrical journal

SFD model with ad-hoc correction factors. As a first step towards an appropriate design of integral SFDs, a finite element program solving the Reynolds equation in each of the squeeze film pads is to be implemented.

Description of test rig and major components

Figure 2 shows the rotor-SFD test apparatus located at the Rotordynamics Laboratory on the main campus of Texas A&M University. The photographs depicts the major components of the rotor and bearing supports housing the dampers. Figure 3 shows a schematic view of the three disk rotor, the bearing and damper supports, and the coupling to a DC drive. Figure 4 shows major dimensions of the test rotor and locations of the displacement sensors for measurement of shaft vibrations. The rotor is supported on two pairs of high precision ball bearings mounted inside the damper journals. The rotor-bearing system rests on a base plate and is isolated from a heavy work table via 1.25 inches (32 mm) thick elastomeric vibration absorbing pad. The test rotor is contained by a safety steel enclosure. The work table weighing 2.4 klb (1,100 kg) rests on 1/4 inch (6.25 mm) thick steel plates and presses a butyl foam rubber isolation pad to the floor of the laboratory.

A 10 HP (7.5 kW) DC power supply and DC motor drive the test rotor. The motor is mounted on elastomeric pads providing vibration isolation from/to the work table. The flexible coupling allows misalignment between the motor and the rotor without exerting side loads. A *drawn cup* roller clutch in the coupling allows the motor to bring the test rotor to a top speed of 9,000 rpm, and then be shut off without applying a torque to the rotating shaft. This feature of the coupling insures free coast down tests of the test rig as the motor drag friction does not affect the rate of rotor deceleration. A DC battery (12 volts, 900 amperes) connected in parallel with the power supply provides a boost in current for start-up acceleration of the test rotor. Initial tests demonstrated that the drive motor could not deliver enough torque to overcome the frictional drag on the test rotor at speeds below 2,000 rpm. The supplementary DC power source is (generally) disconnected when the rotor reaches a speed of 5,000 rpm or it can be left connected for recharging using the remnant power from the main power supply.

The test rotor is a 26.5 inches (673 mm) long shaft of main diameter equal to 3 inches (7.62 mm) as shown in Figure 4. The drive end, 7 inch (177.8 mm) long, and free end, 5.5 inch (139.7 mm) long, are of a diameter equal to 0.99 inches (24 mm) where the ball bearings are inserted. The shaft contains three 1 inch (25.4 mm) thick disks shrunk fit at evenly spaced intervals of 2.5 inches (63.5 mm). Two of the disks are of 11 inches (279.4 mm) diameter, and the third is 9 inches (228.6 mm) diameter. The weight of the rotor alone is 92 pounds (41.7 kg) and does not include the damper journal weights or the coupling to the drive motor. Each disk has 10-32 threaded holes spaced 30° apart and at radii equal to 4.5 inches (large disks) and 3.5 inches (small disk). At these locations, calibrated imbalance masses are inserted prior to dynamic testing. The residual rotor imbalance has been determined to be 0.008 oz-in (0.58 g-cm) as certified from an independent balancing facility.

The rotor is supported on two pairs of high precision ball bearings. A thin spacer ring separates the ball bearing pairs. A nut and collar allows the application of a preload on each bearing pair at a recommended torque equal to 200 lb-in (22.6 N-m). The nominal ball bearing length is 0.35 inches (9 mm)., and 1.6535 inches (42 mm) O.D. and 0.9843 inches (25 mm) I.D. Lubrication to the ball bearings is drawn from the flow through the damper film lands via a radial hole of 1/16 inch (1.6 mm) diameter discharging to the annular space between the ball bearings.

The bearing support housings are split elements with a 1.42 inches (36 mm) wide groove at mid length of their inner bore. This groove is the seat for the damper housings, and on installation of each damper bearing, it becomes a circumferential chamber that allows lubricant feeding to the damper film lands and ball bearings. A lubricant feed port is located on the side (horizontal plane) of the support, and ports at the bottom sides collect the oil discharge from the ball bearings and squeeze film elements. One (outside) face of the support housings holds the displacement sensors. The other face holds the elastic structure for support and centering of the conventional squeeze film dampers.

The test apparatus has been designed to hold two types of squeeze film dampers, namely a conventional SFD and an integral SFD. The conventional damper requires of a **soft** centering structural mechanism (squirrel cage), and its implementation demanded additional pieces and elements adapted to the support housings (see Figure 1a).

The conventional damper, depicted in Figure 5, consists of a cylindrical housing and a journal. The damper housing rests on the groove of the split bearing support and contains six feed holes of 1/16 inch (1.6 mm) diameter connecting the circumferential groove to the damper squeeze film lands. The journal is of diameter (D) and length (L) equal to 3.72 inches (95 mm) and 0.91 inches (23.0 mm), respectively. The journal inner bore holds the ball bearings which connect the damper to the rotating shaft. The journal contains also a port for installation of a pressure transducer facing the middle plane at the bottom of the circumferential squeeze film land. The nominal radial clearance (C) on the damper film lands is equal to 0.009 inches (0.229 mm). Note that the damper slenderness ratio, (L/D), and clearance to journal radius, (2.C/D), are equal to 0.243 and 0.005, respectively. These parameter values reproduce current damper applications in aircraft engines. The journal is connected to the bearing support with four steel rods of 0.235 inch (6 mm) diameter and 1.97 inches (50.2 mm) length. The support is designed for a nominal radial stiffness $\mathbf{k_s = 20{,}000\ lb/in\ (3.5\ MN/m).}$ Alignment and centering of the damper journal within its housing is provided by four fine positioning screws mounted on brackets also attached to the bearing support.

The damper housings also include provisions for the installation of end seals on their axial faces. These end seals in the form of thin steel rings allow a controlled gap at the lubricant exit planes, and their function is to restrict the flow rate through the damper sections and increase the squeeze film forces. Room temperature measurements [70°F (21°C)] of the damper film clearance

during the journal centering process have shown that this radial clearance (C) is actually equal to 0.0078 inches and 0.0096 inches (0.198 mm and 0.244 mm) in the horizontal and vertical directions, respectively for the damper installed at the rotor free end. The measured clearances for the damper facing the motor drive are equal to 0.0077 inches (horizontal) and 0.0093 inches (vertical). The distortion of the damper clearance may be due to compression exerted when fastening the bearing top supports.

The integral flexure-pad SFD shown in Figure 6 consists of four 55 ° arcuate squeeze film pads which incorporate S-shape thin elastic webs providing the journal support radial stiffness. The squeeze film lands are at a diameter (D) of 3.8 inches (96.52 mm) and have an axial length (L) equal to 0.91 inches (23.0 mm). The nominal journal web support stiffness is equal to 20,000 lb/in (3.5 MN/m) and the operating film thickness of the squeeze film pads is designed to be 0.011 inches (0.280 mm). To achieve these film clearance the top and bottom pads have been machined to 0.0085 and 0.0135 inches (0.216 and 0.343 mm), respectively, so that under the static deflection due to the rotor weight they increase (decrease) to the desired nominal clearance. Each squeeze film pad is fed directly from the supply groove through a 1/16 inch (1.6 mm) hole located at the middle plane of each pad. The integral SFD also has a port for direct lubrication of the ball bearings and a port for installation of a pressure transducer facing the middle plane of the bottom squeeze film land.

The lubrication system shown schematically in Figure 7 delivers oil to the bearing housings from a 40 gallon (151 liters) reservoir through a variable frequency (1 HP, 5 GPM) gear pump. The temperature in the reservoir is controlled using a 1.5 kW electrical heater able to raise the reservoir oil temperature about 50° F (28 °C) in approximately 2 hours .The lubricant discharged from the bearing supports flows through a forced air convection cooler with a thermostat control, and then it is pumped back to the main reservoir. The oil supply and return lines have a number of control valves and incorporate a flow meter and pressure gauges. The main feed groove to the damper film lands branches to additional ports for direct delivery of lubricant to the ball bearings without this first passing through the squeeze film dampers.

Figure 8 shows a schematic view of the principal instruments attached to the test rig. A turbine flowmeter displays the flow supplied to the bearing supports and Bourdon-type pressure gauges indicate the static supply pressure to each squeeze film damper. Three pairs of non-contact eddy-current displacement sensors (PP) are mounted to measure directly the rotor displacements at locations next to the damper on the motor drive end, the middle disk, and the damper at the rotor free end. The displacement sensors are mounted in the horizontal and vertical directions. Piezoelectric dynamic pressure sensors (PT) are installed at the bottom of the middle section of the damper journals (see Figures 5 and 6). An optical keyphasor ($K\Phi$) facing the drive motor coupling detects the rotor speed. Piezoelectric accelerometers with magnetic bases are also mounted on the bearing supports and the base plate. Temperature measurements are performed with type-K thermocouples (TT) at several locations on the test rig. These are namely, at the

pump discharge and return lines of the lubrication system, on the drive motor, and room temperature. Most importantly, thermocouples cold welded to the side faces of the damper housing provide direct measurements of the operating temperature at the discharge sections of the damper squeeze film lands. Table 1 provides a summary of the sensors attached to the test apparatus and displays information on their sensitivity and notation for use in the data analysis process. Appendices A and B provide full details and the cost of all the equipment components and instrumentation

An eight-channel simultaneous sampling 20 kHz data acquisition interface unit records signals from the six displacement sensors and the two pressure transducers, and an additional channel senses the signal from the optical rotor speed KΦ sensor. The acquisition system is specifically tailored for measurements in rotating machinery and includes slow-roll subtraction, order-tracking and synchronous response filtering. The PC Windows based computer data acquisition software offers a multitude of options for measurements and presentation of test results including rotor orbits, Bode and Nyquist plots, and FFTs. An instrumentation console contains digital displays of the operating rotor speed, flow rate, supply and damper discharge temperatures, and includes the controls for operation of the lubrication pumps and the oil cooling and heating elements. Three oscilloscopes display the rotor orbits at the measurement locations, a fourth oscilloscope shows the SFD dynamic pressures, and a frequency analyzer depicts the FFT of selected vibration signals.

Rotordynamics model and system parameters identification

XLRotor, a linear rotordynamics software package based on the transfer matrix method, is used for prediction of the rotor system natural frequencies, mode shapes and imbalance response. The test rotor is modeled using 38 stations as shown in Figure 9 with the drive end located at the left of the graph. The measured rotor weight including the conventional SFD journals is 98 lb (44.5 kg) using a scale. The manufacturer provides the weight of the coupling as 7.6 lb (3.45 kg). The model indicates a total rotor weight of 101 lb (45.8 kg) incorporating only half the coupling weight. The estimated center of mass of the rotor-bearing system is located 13.1 inches (333 mm) from the drive end. The bearing supports are located at stations 7 and 33 which incorporate the added masses of the damper journals. Also station 1 includes the added mass and moments of inertia of the coupling.

Identification of rotor free-free modes

The rotor (shaft and press fitted disks) was hanged with nylon ropes for identification of its elastic unconstrained modes. A miniature (1 gram) piezoelectric accelerometer was installed at different locations along the rotor, and subsequently, the rotor was excited in the horizontal direction with a calibrated impulse hammer. The measurements show two distinct natural frequencies as given on Table 2 which also includes the predictions from the model and the percent difference in the estimation of these natural frequencies. The correlation of the predicted

and measured free-free mode natural frequencies validates the structural model. Note that the measurements and predictions did not include the damper journal and coupling masses.

Measurement of conventional damper lateral support stiffness

At the time of this writing the conventional SFDs are currently installed on the test apparatus. Precise knowledge of the "squirrel cage" support lateral stiffness is needed for accurate determination of the rotor-bearing critical speeds. To this end, each damper journal and its four flexural rods were assembled and rigidly connected to the bearing supports. All parts were weighed before assembly. Two methods were used for measurement of the damper lateral stiffness. *Method (a)* consisted of loading the damper journal and then measuring the journal deflection using a dial gauge. A lever arm with a mechanical advantage 5:1 was used to transmit the applied loads in the vertical direction, while horizontal loads were exerted using a rope and calibrated scale to pull on the journal. *Method (b)* was based on impacting the damper journal with a calibrated piezoelectric load hammer and measuring the ensuing vibration with a miniature (1gram) piezoelectric accelerometer. The second method has the advantages of providing an indication of the structural damping of the elastic support, and it also allowed for load excitations to be delivered and measurements to be collected at different circumferential locations around the damper housing.

A summary of the measurements is provided in Table 3 for the damper journals designated as (1) close to the rotor free end, and (2) facing the drive motor end. The test results demonstrate that the radial stiffness did not vary greatly at different circumferential locations. The load-displacement method shows reliable results as evidenced by the correlation coefficients (0.98 and higher) of the test data. The second method shows different results because it requires the evaluation of the *equivalent mass* of the damper journal and flexure bars. Note that a 4% increase in the mass for the drive end bar supports would have brought identical stiffnesses from the two methods. The tests also indicate that the small structural damping from the supports will provide a negligible influence on the rotor-bearing system response.

Measurement of integral damper flexural support stiffness

The integral flexure-pad squeeze film dampers have been constructed and at this time experiments are being performed to determine the stiffness of each pad as well as of the entire damper. Geometric measurements have shown that the pad clearances are uneven and ranging from 0.008 to 0.011 inches (0.203 to 0.280 mm) as designed. A special fixture is under construction for applying loads and measuring the pad deflections to determine the support stiffness.

Identification of natural frequencies for the test rotor-bearing system

The rotor supported on the conventional dampers was excited with a calibrated impact hammer at the coupling (most sensitive to manifest the elastic modes) and the rotor motion was measured with a small piezoelectric accelerometer attached magnetically to the middle-disk. The system was free of any lubricant. A typical frequency response spectrum of the accelerometer for

motion in the vertical direction is shown in Figure 10. The results indicate natural frequencies at 60, 100, 200 and 888 Hz with an uncertainty of +/-4 Hz. Other tests performed with impact excitation and acceleration measurements at the same rotor location show similar results. The FFT of the latter tests used a maximum frequency span of 500 Hz to render measurements with less uncertainty (+/- 2 Hz).

Table 4 presents a summary of the measurements and the predictions from ***XLrotor***. The rotordynamic model requires values of the bearing stiffness which were set to K_{XX}=K_{YY}=20,420 lb/in (3.55 MN/m) for the drive end (station 9) and K_{XX}=K_{YY}=18,421 lb/in (3.21 MN/m) for the free rotor end (station 33) as given by the load-displacement tests detailed above. No cross-coupled stiffness values were included. The computational predictions have been calculated for very light damping coefficients C_{XX}=C_{YY}=3.2 lb-s/in (557.5 N-s/m) at each bearing support.

Figure 11 (a-b) displays the first two natural modes corresponding to a cylindrical and conical modes, respectively, while Figure 11 (c) shows the first bending rotor mode. The correlation of predictions with measurements is satisfactory, although some differences are relevant for discussion. First, the test rotor shows clearly different vertical (f_{Vn}=62 Hz) and horizontal (f_{Hn}=56 Hz) fundamental natural frequencies demonstrating that the bearing split supports are softer in the horizontal direction. On the other hand, the addition of the flexible coupling at the rotor end determines a dramatic reduction of the first elastic mode from 630 Hz (see results from Table 2) to just 200 Hz. This result is easily explained since the overhung drive end is the greatest contributor for the motion in the third natural mode (see Figure 11c).

The first mode (cylindrical) indicates a rotor motion very close to a rigid body mode. An equivalent system stiffness and critical damping coefficients are thus likely to be found. Using a system mass M_{eq}=101 lb (45.8 kg) and the measured fundamental natural frequencies (f_n) of 62 Hz (vertical) and 56 Hz (horizontal), determines the equivalent parameters for the fundamental mode as:

Vertical direction

$K_{Veq} = (f_{Vn}\, 2\pi)^2 (M_{eq}) = 39.666$ klb/in (6.94 MN/m) $\qquad C_{Vcrit} = 2 (K_{Veq}\, M_{eq})^{1/2} = 203.6$ lb-s/in (35.6 KN-s/m) $\qquad$ (1)

Horizontal direction

$K_{Heq} = (f_{Hn}\, 2\pi)^2 (M_{eq}) = 32.361$ klb/in (6.94 MN/m) $\qquad C_{Hcrit} = 2 (K_{Heq}\, M_{eq})^{1/2} = 184.0$ lb-s/in (32.2 KN-s/m) $\qquad$ (2)

with an uncertainty of +/- 1 klb/in (0.17 MN/m).

The equivalent stiffness in the vertical direction is very close to the sum of the measured support stiffnesses, 20.420 klb/in (drive end) and 18.421 klb/in (free end), respectively. The reduced equivalent stiffness in the horizontal direction (16 % less than the measured compound value of

38.85 klb/in) can not be readily explained. However, it is noted that the fundamental mode of vibration shows motions at the drive end slightly larger than at the free end.

The test rotor supported on conventional SFDs with flexure bar centering structures is currently operational. The fluid initially selected to lubricate the ball bearings and squeeze film dampers was an ISO VG 32 oil which (unfortunately) produced a too well damped response while passing through the system first critical speed (approximately 3,600 rpm). That is, the rotor showed small amplitudes of motion even with large levels of imbalance. It is important to note that the **damper design** was carried out using the direct damping coefficient formulae for the open ends SFD with a π-film cavitation extent model. The tests have since then proved the SFD damping values to be much larger than predicted. Furthermore, there are no traces of dynamic cavitation on the measured pressure signals for most operating conditions. The lesson learned from this experience is that the indiscriminate application of theoretical formulae can lead to poor or limited designs.

At the time of this writing, the lubricant has been replaced by an ISO VG 10 oil with a lower viscosity. More details on the phenomena observed and problems encountered while the test-rotor operated to a maximum speed of 8,800 rpm (and higher) are given later. The viscosity of the two lubricants used to date was measured at an independent facility. The viscosity values are given in Table 5. The tests performed on a rotating spindle meter also indicate the oils to be insensitive to shear rate variations, thus confirming their Newtonian character.

Measurement of system damping at zero rotational speed

Oil was circulated through the lubrication system, the squeeze film dampers and ball bearings. The rotor was then excited with a calibrated impact hammer and the rotor motion was measured with a small piezoelectric accelerometer magnetically attached to the center disk. Transfer functions of acceleration versus load were obtained using a frequency analyzer, and from these, values for the system damping coefficient were evaluated. Prior to the tests, the lubricant in the reservoir was heated to a preset temperature; and then, the tests were conducted with the oil circulating through the SFDs with a pressure supply equal to 10 psig (0.7 bars). Impulse excitations at the mid disk revealed a frequency response with a single peak at the fundamental (rigid body) mode. On the other hand, impulses at the other disks excited also the conical and first bending modes.

A full set of tests with the ISO VG 32 oil were found to be erroneous due to an improper use of the frequency analyzer when setting a narrow window of just 250 Hz. In addition, excessive amplification factors were selected for the transducers which (most likely) saturated the transducer signals bringing unreliable results. Note that these tests provided an estimate of the system damping coefficient on the order of 24 lb-s/in (4.2 kN-s/m) which was close to the design value, and rendered a system damping ratio (ξ) equal to 0.10. However, the imbalance responses showed very well damped responses which prompted the change to a lighter viscosity lubricant .

Recent tests with the lighter oil (ISO VG 10) have been more successful. Careful attention to the details has been the norm in these last measurements. The identified values of system damping coefficients for the fundamental mode are reported in Table 6. These coefficients represent the averages of at least 6 impact tests. Factors influencing the measurements and their repeatability include excessive wear of the impact hammer tips and difficulty in imparting the loads in the desired directions (particularly for the horizontal plane). Table 6 also includes predictions for the system damping as the sum of each SFD damping coefficient. The theoretical damping coefficient is calculated for a short length-open ends SFD at the centered position and without fluid cavitation. The formulae used is then

$$C_{SFD} = \pi\mu\,(D/2)\,(L/C_*)^3\,/(1-\varepsilon^2)^{1.5} \qquad (3)$$

where D,L and C_* denote the SFD diameter, length and nominal clearance, respectively; and, the fluid viscosity is determined from the measured temperature at the SFD discharge plane.$\varepsilon = e/C_*$ corresponds to the journal orbit radii taken as zero for the predictions.

The measurements indicate a slight increase in the damped natural frequencies, and the identified damping values do not correlate well with the theoretical predictions for a centered SFD. Note that the experimental values include not only the dampers' damping but also the damping from other sources like the lip seals, coupling, etc. Furthermore, the system damping coefficient (C_H) for horizontal motions is much smaller than the one in the vertical direction (C_V). It is likely that the impulse excitations in the horizontal plane had a large degree of uncertainty. This assertion was later verified when controlled imbalance coast-down tests were performed.

At the time of this writing the residual system damping (w/o lubricant in the dampers) is not well known since early experiments aimed to determine this parameter have been found to be in error. The authors believe the residual damping value (i.e. no oil on the test apparatus) could be as low as 12 lb-sec/in and as large as 24 lb-sec/in (2.1 to 4.2 KN-s/m). Planned tests will attempt to determine this coefficient with reasonable degrees of certainty and repeatability.

If the residual damping coefficient is regarded as a known value, say 12 lb-sec/in at 80 °F for example, then the identified vertical damping values agree reasonably well with theory. Nevertheless at this temperature, the measured damping ratios $\xi = C/C_{crit}$ are equal to 0.155 and 0.206, in the horizontal and vertical directions, respectively (see Table 6). Related to these values, the amplification factors ($Q = 1/2\xi$) for the fundamental mode are just 3.22 and 2.42, respectively.

Operation and troubleshooting of the test rig

The test rig has been in service since the beginning of 1996. Rotordynamic tests have consisted of accelerating the rotor to approximately 8,000 rpm, then controlling the DC power source, and allowing the system to decelerate slowly till rest. The data acquisition system has been configured to automatically perform measurements of the shaft displacement and SFD pressure

while the system comes to its top speed and then decelerates to a stop. Graphical display of the shaft vertical displacement versus rotational speed in unfiltered and 1-X filtered modes are displayed in real time on the computer screen. The following is a brief list of the major problems encountered on the operation of the test apparatus.

1) It became evident that the DC power supply could not deliver enough current to turn the rotor with an acceptable acceleration rate. The acquisition of a booster DC battery connected in parallel with the main DC source fixed the problem. However, in this later case the acceleration rate is too fast and care needs to be exercised when operating the apparatus.
2) The installation of a faulty cable connecting the pressure transducer located on the drive end damper caused this sensor to become inoperative. Accessibility to this sensor is not possible without removing the displacement sensors and the top half of the bearing supports. The remedial procedure was considered too complicated since it would have required recentering the damper journals within their housings. Thus, to this date the drive-end pressure sensor is inoperative.
3) The test rig was brought to speeds close to 10,000 rpm and the baseline vibration response was recorded. The measurements demonstrated the rotor to be well balanced. However, the slow roll was of significance and approximately equal to 0.0015 inches (0.038 mm).
4) Imbalance masses were inserted at the middle disk and the rotor synchronous response was subsequently measured. First, data acquisition glitches from the commercial software were evident in some of the tests. The problem resides in that sometimes the keyphasor signal is "mysteriously" lost for some of the measured channels and this causes erratic 1-X filtered responses. The supplier of the hardware/software is currently reviewing this unusual test data. Second, and most importantly, careful observation of the rotor displacements in the oscilloscopes revealed that the shaft centerline changed dramatically from its initial position to a different one at the end of a given test. Thus, the shaft showed a severe thermal bow amounting to approximately 0.0024 inches (0.061 mm) at the middle disk and 0.002 inches (0.051 mm) at the damper supports. Measurements of the shaft surface temperature at the disk locations as well as closer to the damper housings were performed. Temperatures at the disks were slightly higher than ambient so excessive windage effects were regarded as unimportant. However, the shaft appeared much hotter at the sides of the support housings, approximately 130°F (73°C) above ambient conditions. This indicated that the shaft overheating came from insufficient lubrication to the ball bearings and presumably excessive preloads to these elements due to the shaft thermal growth.

Subsequent tests have been conducted with lubricant delivery pressures of 1 bar (15 psig) to warrant enough flow through the bearing supports. In addition, long periods of shaft warm-up (approximately 45 minutes) at a rotational speed of 3,000 rpm are needed before actual testing. The remedial procedure has demonstrated the shaft temperatures to be just a few degrees above the operating temperature of the lubricant, and the measurements indicate minimal rotor thermal bow between the initial and final stages of a test. However, the excessive lubrication sometimes overflows the bearing supports and oil leaks to the base plate. The waste lubricant under the disks

is then "blown away" by the air drag action of the rotating disks creating a large oil spill area in the Laboratory floor. An "oil catcher" structure attached to the protective frame has been constructed to contain as much as possible this environmental problem. However, this "oil catcher" structure impairs air circulation, and hence, the entire rotor easily warms up again !.

Test rig synchronous imbalance responses

Small calibrated masses (m) were added to the middle disk (at a radius r= 4.5 inch [114.3 mm]). The warm rotor was then brought rapidly to a top speed of approximately 9,000 rpm, the power shut down, and the coast-down response was measured. Table 7 provides a summary of the test peak-to-peak amplitudes of synchronous response at the locations of measurement and while passing through the first critical speed. The table includes the lubricant temperature and the imbalance displacement u calculated equal to $[m_{\times}r/M_{eq}]$. All experiments were conducted with a pressure supply to the SFDs equal to 15 psig (1 bar).

Each experimental coast-down was repeated twice to verify the repeatability of the tests. Note that the tests with the larger imbalance masses were performed at lower lubricant temperatures. Figures 12, 13 and 14 depict the (vertical and horizontal) synchronous rotor responses at the locations of measurement on the rotor drive end, near the middle disk and the free end, respectively. (Refer to Figure 4 for a description of the displacement sensor locations). The highest speed for the test with the largest imbalance mass (m.r= 148.5 gr-in, u=83 μm) was 5,300 rpm. Continuation of the test at higher speeds was not considered safe for the test apparatus and the operator.

The measurements show rotor amplitudes of motion proportional to the unbalance masses and make evident the passage through the first two critical speeds. The cylindrical critical speeds are approximately 3,100 rpm and 3,800 rpm, for the horizontal and vertical directions, respectively, while the forward conical critical speed is around 7,000 to 8,000 rpm. Note that the critical speeds do not shift as the rotor imbalance increases. Excitation of the conical critical speed was thought unlikely since the imbalance masses were located at the middle disk (very close to the rotor mass center). It is important to note that while passing through the forward-mode conical critical speed the response at the middle disk showed a frequency component equal to twice the rotational speed and with a magnitude slightly smaller to that of the synchronous frequency.

At this time only the rotor responses through the cylindrical mode (critical speed) have been analyzed with some detail. It is noted from Table 7 that the average results from the three measurements are very similar to the amplitudes near the middle disk. Figure 15 shows these rotor amplitudes near the middle disk to be nearly proportional to the unbalance displacement (u). These results then demonstrate the SFDs to be operating as linear mechanical elements. The system amplification factor (Q) at the first critical speed is easily determined by the ratio of the rotor amplitude of motion to the unbalance displacement (u). From this result, values of the system damping ratio ($\xi=1/2Q$) are also extracted. Finally, system damping coefficients are also

determined by multiplying ξ times the critical damping coefficient. Table 8 provides a summary of the Q, ξ , and damping coefficients identified from the measured average rotor amplitude of motion. The results also include the maximum amplitude of motion (at the drive end) divided by a nominal SFD radial clearance (C_*=8.7 mils [0.222 mm]) to highlight the magnitude of the journal displacements within the damper clearance.

The results obtained (Table 8) establish a linear operation of the SFDs at the first critical speed in spite of the large journal amplitudes at the drive end SFD of up to 69% of the nominal radial clearance. Figure 16, based on the values of Table 8, shows similar system damping coefficients in the vertical and horizontal directions. These results agree well with the impact excitation test values in the vertical direction (see Table 6). The test damping coefficients do not vary (as expected from theory) greatly with the amplitude of rotor motion. The larger damping coefficients for the tests with the largest imbalances are probably due to the lower oil temperature rather than a direct consequence of the rotor's large amplitude motions.

Theoretical damping coefficients based on the full film SFD open ends model (see equation 3) do not agree with the measurements. In general predicted damping coefficients increase rapidly (non-linearly) with the rotor amplitude of motion (See Figure 16). Predicted values of system damping, equal to two times the theoretical damping coefficient (C_{SFD}), are 18 lb-sec/in (3.15 kN-sec/m) for a centered journal (ε=0) and as large as 36 lb-sec/in (6.3 kN-sec/m) for a journal amplitude of motion equal to 60% of the radial clearance.

The measurements of squeeze film pressures at the drive end damper show no indications of lubricant cavitation in any of the tests. Figure 17 shows the amplitudes of p-p pressure for the coast-down test with largest imbalance (i.e. 148.5 gr-in, u=0.083 mm). The maximum peak-to-peak dynamic pressure is about 1.7 bars (25 psi) while passing through the critical speed. Other test with a smaller unbalance (u=0.071 mm) shows the dynamic pressure to increase as the rotor speed rises to its top value (9,000 rpm) and with a magnitude as large as 2.5 bars (37 psi)

A unique test was performed to verify the benefit of the SFD supports on the response of the rotor. An unbalance mass of 14.7 grams was inserted on the disk closest to the free end (r=3.5 inch, u=28.5 μm). Figure 18 shows the rotor synchronous response near the middle disk for a run-up to 5,000 rpm without any lubricant supply to the damper, then the pump was turned on and lubricant was delivered at a pressure of 10 psig (0.7 bars) and at a temperature of 79 °F (26.1 °C). The coast-down curve shows the response with the SFDs active, i.e. full of lubricant. The large differences in responses for the coast-up without lubricant and the coast-down are dramatic and demonstrate the action of the SFDs. From this test and at the passage through the first critical speed, system damping ratios (ξ) for dampers inactive and active are estimated to be 0.12 and 0.28, respectively. The damping ratio for the active SFDs is larger than for the tests presented in Table 7 since the lubricant is at a lower temperature, and its viscosity is larger (approximately 14.9 centipoise). Note that the damping ratio for the inactive SFDs is still large since some

remnant lubricant was still within the dampers' thin film lands. This assertion was verified when noting that the (SFD free end) pressure sensor showed substantial film pressures when the rotor traversed the first critical speed. Figure 19 depicts dramatically the measured pressures with no oil circulating and with oil flowing through the dampers (coast-down). Note that larger pressures are generated in the "no oil" condition demonstrating that just a few drops of lubricant are able to attenuate the rotor vibrations.

The rotor dynamic analysis of the test apparatus continues. Damped eigenvalues have been calculated with speed invariant damping coefficients equal to 23 lb-sec/in (4.02 kN-sec/m) at each bearing support. Figure 20 displays the predicted damped natural frequencies versus rotor speed. The results obtained verify the measurements and demonstrate the close proximity between the first two rigid body critical speeds (cylindrical and forward-conical) and also the appearance of the first bending mode at just 10,000 rpm. The predictions then explain the large amplitudes of rotor response at the free-end which keep increasing after 7,000 rpm.

Analysis of integral SFDs

The analysis of integral SFDs must couple structural and hydrodynamic models for simultaneous evaluation of the elastic forces in the support web structure and the fluid film forces developed on each squeeze film pad. The dynamic force response of the integral damper to shaft motions also depends on the way the ball bearing outer race fits within the damper journal. A very tight fit makes the journal and ball bearing(s) move as a single element but it may cause excessive interference loads on the rolling elements. This could be aggravated more if material compatibility for even thermal growth (of journal and ball bearing) are not effectively accounted for. A looser fit or contact between the journal and ball bearing at selected zones may cause undesirable dry friction forces which may even cause stick-slip phenomena at certain frequencies of operation.

Detailed analysis of integral SFDs is therefore not a simple task. As a first step towards building a general model it is necessary to develop a hydrodynamics model to calculate fluid film forces due to the squeeze film motion of each pad. Let a Newtonian, incompressible and isoviscous (μ) fluid flow within a thin gap (h) enclosed between a rigid housing and a moving upper pad. For inertialess flows, Reynolds equation describes the generation of hydrodynamic pressure (P) as:

$$\frac{\partial}{R\partial\theta}\left(\frac{h^3}{12\mu}\frac{\partial P}{R\partial\theta}\right)+\frac{\partial}{\partial z}\left(\frac{h^3}{12\mu}\frac{\partial P}{\partial z}\right)=\frac{\partial h}{\partial t} \qquad (4)$$

In this equation, (θ,z) correspond to the circumferential and axial coordinates along the pad, and dh/dt denotes the time rate of change of the film thickness, i.e. a local squeeze film velocity.

The squeeze film pad is fed through holes located at mid-arc length or at the sides of the pad. Here the pressure is regarded as equal to the supply pressure from the delivery system. End

seals (in the form of thin rings) are attached to the faces of the damper bearing. A local relationship between the axial flow and the pressure drop across the seal is modeled as (San Andres and Vance, 1987):

$$q_z = \left(\frac{g^3}{12\mu l}\right)\left[P_e - P_a\right] = C_L\left[P_e - P_a\right] \qquad (5)$$

where g and *l* denote the end seal gap and radial extent, respectively. Pe and Pa correspond to the exit damper discharge and ambient pressures, and C_L is a local end seal coefficient with physical units of $[m^2s^{-1}Pa^{-1}]$. Note that the open end condition is obtained for C_L large while the no end leakage condition is attained for C_L=0.

A finite element program, based on an earlier code by San Andres (1994), has been modified to solve equations (1-2) for an integral damper with a number of squeeze pads each with a different nominal clearance. The current film thickness model h(θ,t) regards the motion of the pads as if rigidly connected to the rolling element bearings simulating a very tight fit. That is, if the rotor moves downward a distance **a,** then the bottom pad moves the same amount squeezing its fluid film, while the top pad also moves downwards **a** and produces an increase in its local film clearance. This simple kinematic model is clearly too restrictive and should be modified over the coming months.

Figure 21 shows computed predictions for the tangential (damping) and radial forces in an integral damper of similar dimensions as the one to be tested. The oil viscosity is 0.013 Pa-sec and the journal motion corresponds to a circular centered orbit with an amplitude equal to 0.140 mm (e/C=0.50) at a whirl frequency of 60 Hz. Maximum dynamic peak-to-peak pressures are just 1.2 bars which do not warrant the initiation of oil cavitation for a pressure supply of 1 bar. The predicted forces have a period equal to ¼ of the journal motion period. This most important feature distinguishes the 4-pad integral SFD from a conventional damper which produces a constant force in the rotating coordinate system whirling at the same frequency as the journal motion. Note also that the integral SFD also provides a periodic radial reaction force even in the absence of lubricant cavitation.

Schedule of work for June 1996-May 1997

The following tasks will be completed:

a) Controlled run-up and coast-down experiments of test-rig with increasingly large values of disk couple imbalances. These tests will be conducted for the conventional SFDs and integral SFDs. Controlled operating parameters include lubricant type and feed pressure and temperatures, and different static SFD journal positions by displacing the flexural centering rods.
b) Correlation of responses for both types of dampers and recommendation of their advantages, disadvantages, etc.

c) Based on measurements of the rotor synchronous response, develop simple and tractable models for the flow field and fluid forces in integral SFDs.
d) Quantification of the system dynamic response in terms of linearity and non-linearity, periodic and aperiodic responses, etc.

Concluding remarks and recommendations

This report provides an account of the development of a test apparatus for measurement of the imbalance response of a rotor-bearing system supported on squeeze film dampers (SFDs). A massive three-disk rotor is supported on high precision ball bearings, and the bearing supports can hold conventional SFDs or integral SFDs. The test apparatus and lubrication systems are fully instrumented, and a data acquisition systems records the rotor motion versus shaft speed at three axial locations and orthogonal planes. In addition, squeeze film pressures are also measured at one of the dampers. The lubrication system allows for oil heating and cooling to vary the viscosity of the lubricant.

The test rig currently houses (conventional) cylindrical SFDs with four-bar elastic supports providing soft bearing mounts and allowing journal centering. Numerous tests have been performed to identify the most important rotor-bearing system parameters. Rotor free-free mode natural frequencies were measured and correlated very well with a transfer-matrix structural model. The stiffness coefficients for the SFD squirrel cage supports were also measured and found to be acceptable and close to the designed value (k_s=3.5 MN/m or 20 klb/in). Measurements of the rotor natural frequencies on its bearing supports show a cylindrical mode (~ 60 Hz), a conical mode (~100 Hz) and a first bending mode (~200 Hz). The first two natural frequencies are within the rotor speed operating range (< 10 krpm), with the conical mode being too close to the cylindrical mode.

Impulse load (rap) excitation of the rotor at null rotational speed and measurements of acceleration allowed the extraction of system damping coefficients from transfer functions. The damping coefficients depend greatly on the lubricant temperature and in generally are much larger than theoretical predictions based on the simple full-film SFD model.

Measurements of the synchronous rotor response with different imbalance weights showed the SFDs to work too effectively (with oil ISO VG 32) with well damped rotor responses for the cylindrical mode of vibration. Further tests with oil ISO VG 10 are currently in progress to study the effect of imbalance location on the rotor response. Rotordynamic analysis are also being performed to predict the measured results.

The rotor synchronous coast-down responses show a linear behavior relative to the magnitude of the unbalance masses inserted at the rotor middle disk. Large SFD journal motions to 70% of the nominal clearance have been measured and with squeeze film pressures as large as 2.5 bars. However, lubricant cavitation has not yet been observed. The system identified damping

coefficients remain relatively constant as the unbalance magnitude increases. Poor correlation exists between the damping coefficients extracted from the tests and theoretical calculations based on the full-film open ends SFD model.

References

Li, X.H., and Taylor, D., 1987, "Nonsynchronous Motion of Squeeze Film Damper Systems," ASME Journal of Tribology, Vol. 109, pp. 169-176.

Mohan, S., and Hahn, E.J., 1974, "Design for Squeeze Film Damper Supports for Rigid Rotors," ASME Journal of Engineering for Industry, Vol. 96, pp. 976-982.

San Andres, L., and J.M. Vance, 1987, "Effect of Fluid Inertia on Finite Length Sealed Squeeze Film Dampers," ASLE Transactions, 30(3), pp. 384-393.

San Andres, L., and J.M. Vance, 1988, "Effect of Fluid Inertia on the Performance of Squeeze Film Damper Supported Rotors," ASME Journal of Engineering for Gas Turbines and Power, Vol. 110, pp. 51-57.

San Andres, L., 1994, "Analysis of Arbitrary Recess Geometry Hydrostatic Bearings," Proceedings of the 6th NASA Conference on Advanced Earth-to-Orbit Propulsion Technology, Huntsville, Alabama, May, NASA CP 3282, Vol. II, pp. 421-430.

Vance, J., 1988, "Rotordynamics of Turbomachinery," John Wiley and Sons.

Zeidan, F.Y., 1995, "Applications of Squeeze Film Dampers", Turbomachinery International, Sept/Oct., pp. 50-53.

List of Tables

Table 1. Instrumentation in NSF-TRC rotor-SFD test apparatus

Transducer	Probe # / gain (mv/mil)	Probe # / gain (mv/mm)	Location *(see figure for map)*
Displacement Probe			
Bearing 1, *Free End*	PP3 / 193.5	7618.11	vertical (0°)
	PP4 / 204.5	8051.18	horizontal (90° L)
Middle	PP5 / 200	7874.02	vertical (0°)
	PP6 / 200	7874.02	horizontal (90° R)
Bearing 2, *Drive End*	PP1 / 205.3	8082.68	vertical (0°)
	PP2 / 200.2	7881.89	horizontal (90° L)
Pressure X-ducer	10.0 mv/psi	147.00 mv/bar	Land of Drive End SFD, (180°)
	5.94 mv/psi	87.32 mv/bar	Land of Free End SFD, (180°)
Thermocouple	0.0225 mv/°F	0.04 mv/°C	Land of Drive End SFD, (0°)
	0.0225 mv/°F	0.04 mv/°C	Land of Drive End SFD, (180°)
	0.0225 mv/°F	0.04 mv/°C	Land of Free End SFD, (0°)
	0.0225 mv/°F	0.04 mv/°C	Land of Free End SFD, (180°)
	0.0225 mv/°F	0.04 mv/°C	DC Motor Casing
	0.0225 mv/°F	0.04 mv/°C	Oil Reservoir

*note: these are raw gains, any amplification will have to be included in the gains separately

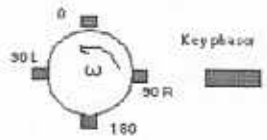

View from Motor

Table 2. Measurements and predictions of free-free modes of test-rotor.
(not including journal and coupling masses).

Mode	Measurement	Model	% difference
1. elastic	630 Hz	622 Hz	-1.3%
2. elastic	930 Hz	941 Hz	+1.2%

uncertainty in measurements is ± 2 Hz

Table 3. Radial stiffness of conventional damper flexible support (squirrel cage) Design value = 20,000 lb/in (3.5 MN/m)

Method	(1) Support free end	(2) Support drive end
(a) Vertical	18,421 lb/in (± 135 lb/in) (3.21 MN/m) (± 0.023 MN/m)	20,420 lb/in (± 160 lb/in) (3.55 MN/m) (± 0.028 MN/m)
Horizontal	18,510 lb/in (± 1020 lb/in) (3.22 MN/m) (± 0.179 MN/m)	20,781 lb/in (± 1174 lb/in) (3.62 MN/m) (± 0.206 MN/m)
(b) Vertical & Horizontal	18,829 lb/in (± 38 lb/in) (3.28 MN/m) (± 0.007 MN/m)	19,684 lb/in (± 39 lb/in) (3.23 MN/m) (± 0.007 MN/m)
natural frequency	254 Hz	260 Hz
equivalent mass	2.86 lb (1.30 kg)	2.85 lb (1.29 kg)
damping ratio ξ	0.012	0.012
structure damping	0.28 lb-s/in (49 N-s/m)	0.29 lb-s/in (50.5 N-s/m)

Table 4. Natural frequencies of test rotor-bearing system. Measurements from rap tests and predictions at zero rotational speed. (No lubricant in bearings).

Mode	Measured Vertical/Horizontal	Predictions	Percent difference
1. Cylindrical	62 Hz / 56 Hz	60.5 Hz	2.5% / 7.0%
2. Conical	100 Hz / 110 Hz	94.5 Hz	5.5 %
3. Elastic$_1$	200 Hz / 204 Hz	194.7 Hz	4.5 %
4. Elastic$_2$	888 Hz (± 2 Hz)	914 Hz	3.0%

Uncertainty in measurements : ± 1 Hz

Predictions based on $K_{XX}=K_{YY}=20{,}420$ lb/in (3.55 MN/m) for the drive end (station 9) and $K_{XX}=K_{YY}=18{,}421$ lb/in for free end, $C_{XX}=C_{YY}=3.2$ lb-s/in (557.5 N-s/m) at both bearing supports.

Table 5. Measured viscosity values of lubricants used in test apparatus

Lubricant type	Specific gravity	Viscosity centipoise	Temperature (°C)
ISO VG 32	0.836	55	25
		41	30
		31	35
		24	40
		15	50
ISO VG 10	0.910	15.8	25.1
		12.8	30
		10.6	35
		8.7	40
		7.8	45
		6.4	50

Table 6. Measured and estimated 1st mode system damping coefficients from Rap tests

Lubricant temperature increases. Lubricant ISO VG 10.

Conventional damper, D=1.86 in (47.2 mm), L=0.9 in (23 mm), C_r = 8.8 mils (0.223 mm).

Oil Temperature °F	Oil Temperature °C	Viscosity centipoise	Theory $2xC_{SFD}$ lb-sec/in	Horizontal C_H lb-sec/in	Vertical C_V lb-sec/in
70	21.1	18.55	34.27	30.63	47.72
80	26.6	14.87	27.47	28.70	42.00
90	32.2	11.86	21.91	27.06	38.80
100	37.7	9.50	17.60	26.50	36.30
104	41.1	8.78	15.31	26.40	34.30
				C_{crit} = 184.0	C_{crit} = 203.6
				f_{Hn} = 58 Hz	f_{Vn} = 64 Hz

Table 7. Summary of rotor synchronous responses at first critical speed. Imbalance at middle disk.

Notation: D: drive end, M:mid disk, F: free end, A: Average, M_{eq}=101 lb (45.8 kg)

Imbalance (gr-in)	Unbalance u (μm)	Vertical P-P (μm) D	M	F	A	Horizontal P-P (μm) D	M	F	A	Temp °F
residual	0.0	24	25	26	25	30	29	26	28.3	99
65.7	36.3	163	155	143	153	147	155	150	150	99
65.7	36.3	162	155	147	154	144	152	148	148	98
104	57.5	248	232	209	230	225	232	224	227	102
104	57.5	249	235	218	234	227	236	228	230	100
128.25	70.9	292	264	242	266	259	265	256	260	96
128.25	70.9	269	242	232	247	248	256	255	253	92
148.5	82.1	307	263	240	270	281	281	275	279	91
Critical Speeds			3500 to 4000 rpm				3100 to 3160 rpm			

Table 8. Amplification factors (Q) and extracted system damping coefficients from rotor synchronous responses at first critical speed. Imbalance at middle disk

C_{Vcrit}=203.6 lb-sec/in C_{Hcrit}=184.0 lb-sec/in

Unbalance u (μm)	u/C	Vertical Amp/C	Q_V	ξ_V	C_V	Horizontal Amp/C	Q_H	ξ_V	C_H	Temp °F
36.3	0.164	0.367	2.09	0.24	48.5	0.331	2.05	0.24	44.8	99
36.3		0.364	2.11	0.24	48.2	0.324	2.01	0.25	45.6	98
57.5	0.259	0.558	1.99	0.25	51.0	0.507	1.97	0.25	46.8	102
57.5		0.560	2.02	0.25	50.0	0.511	2.00	0.25	46.1	100
70.9	0.319	0.657	1.856	0.27	54.67	0.583	1.814	0.28	50.7	96
70.9		0.606	1.728	0.29	58.7	0.559	1.765	0.28	52.1	92
82.1	0.370	0.691	1.625	0.31	62.40	0.632	1.680	0.297	54.7	91
	C=0.222mm				lb-sec/in				lb-sec/in	

List of Figures

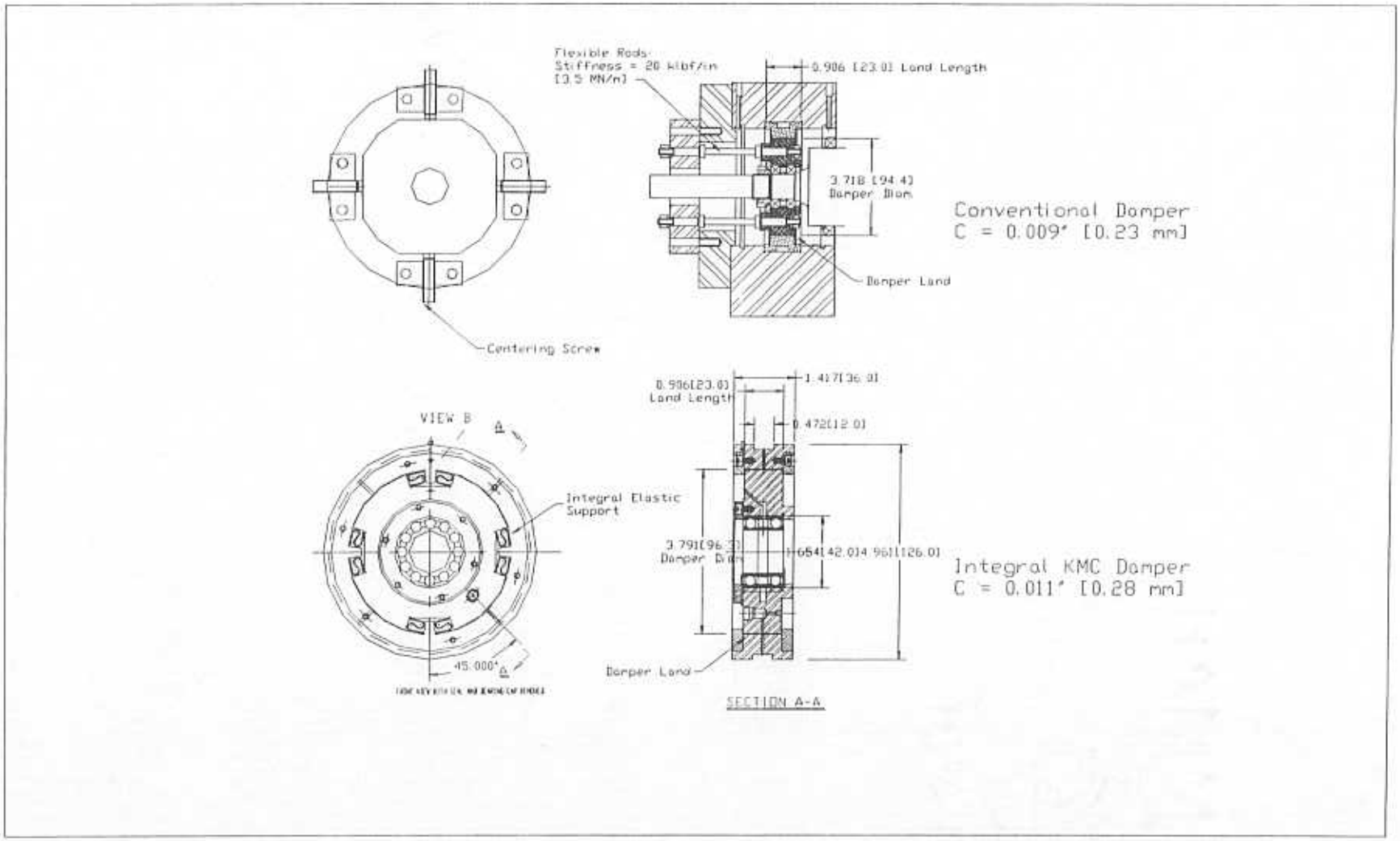

Figure 1. a) Conventional Cylindrical Squeeze Film Damper and elastic support
b) Integral KMC Squeeze Film Damper

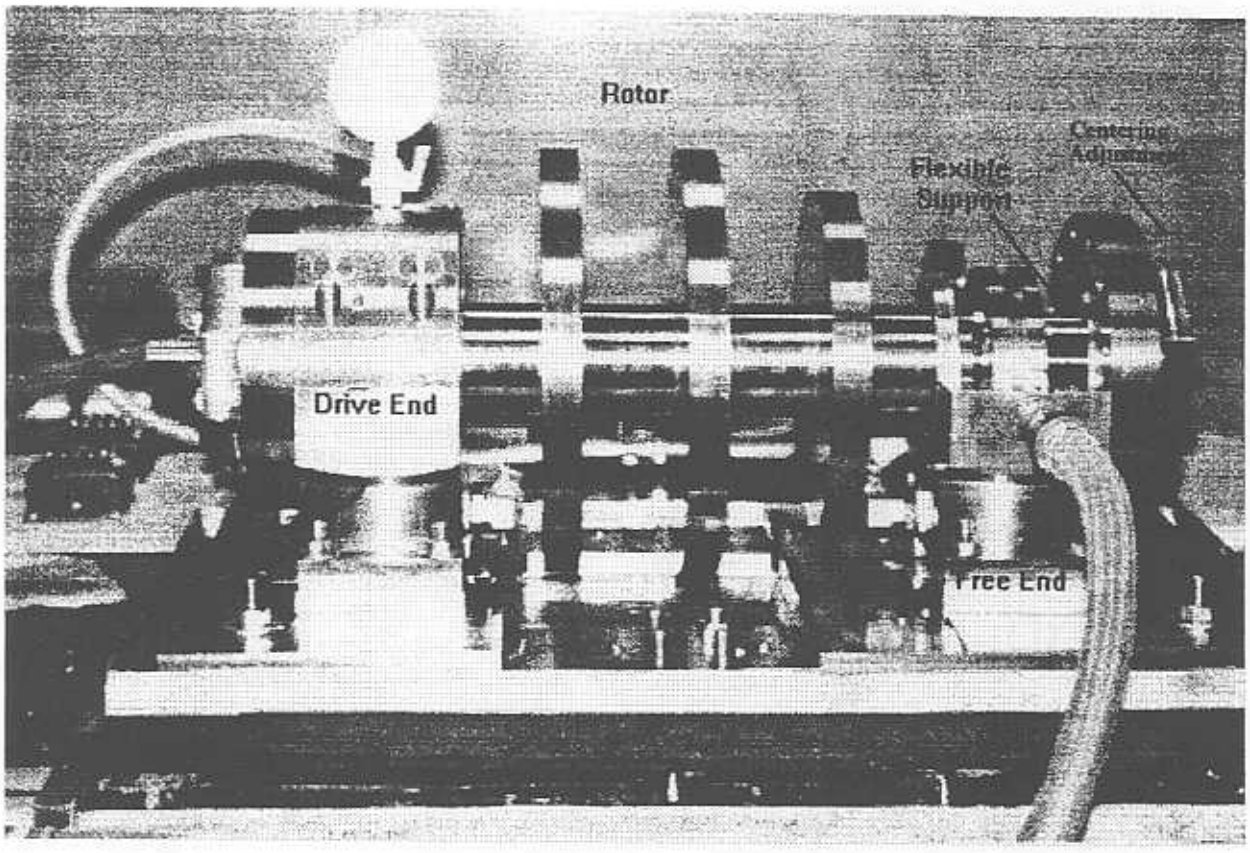

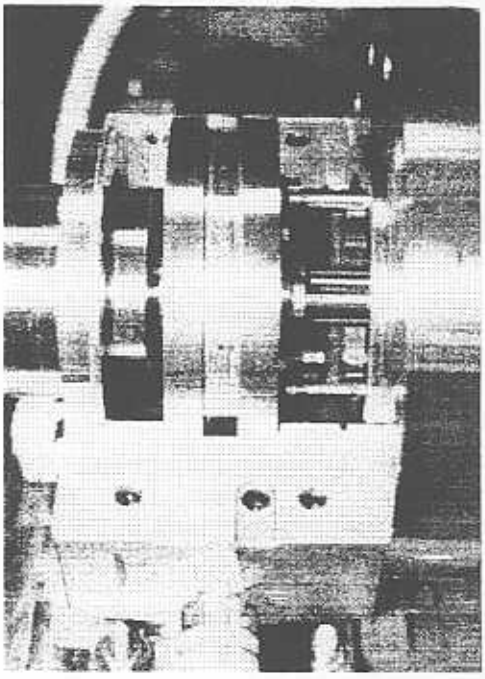

Figure 2: Photograph of Test Rig Showing Open Bearing Support and Centering Mechanism and Flexible Support; Closeup of Open Bearing Support

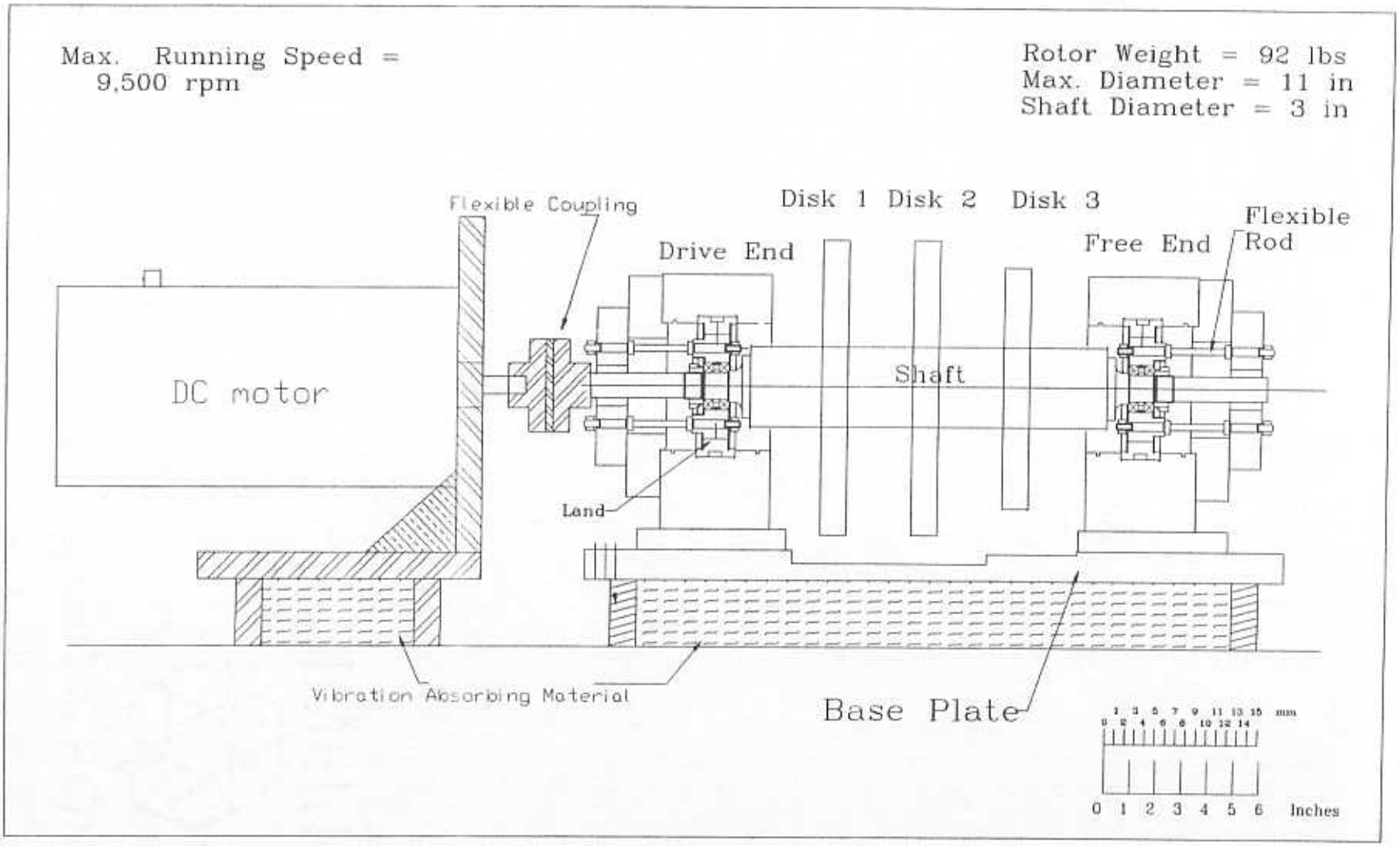

Figure 3. Schematic View of Test Apparatus with Conventional Squeeze Film Dampers

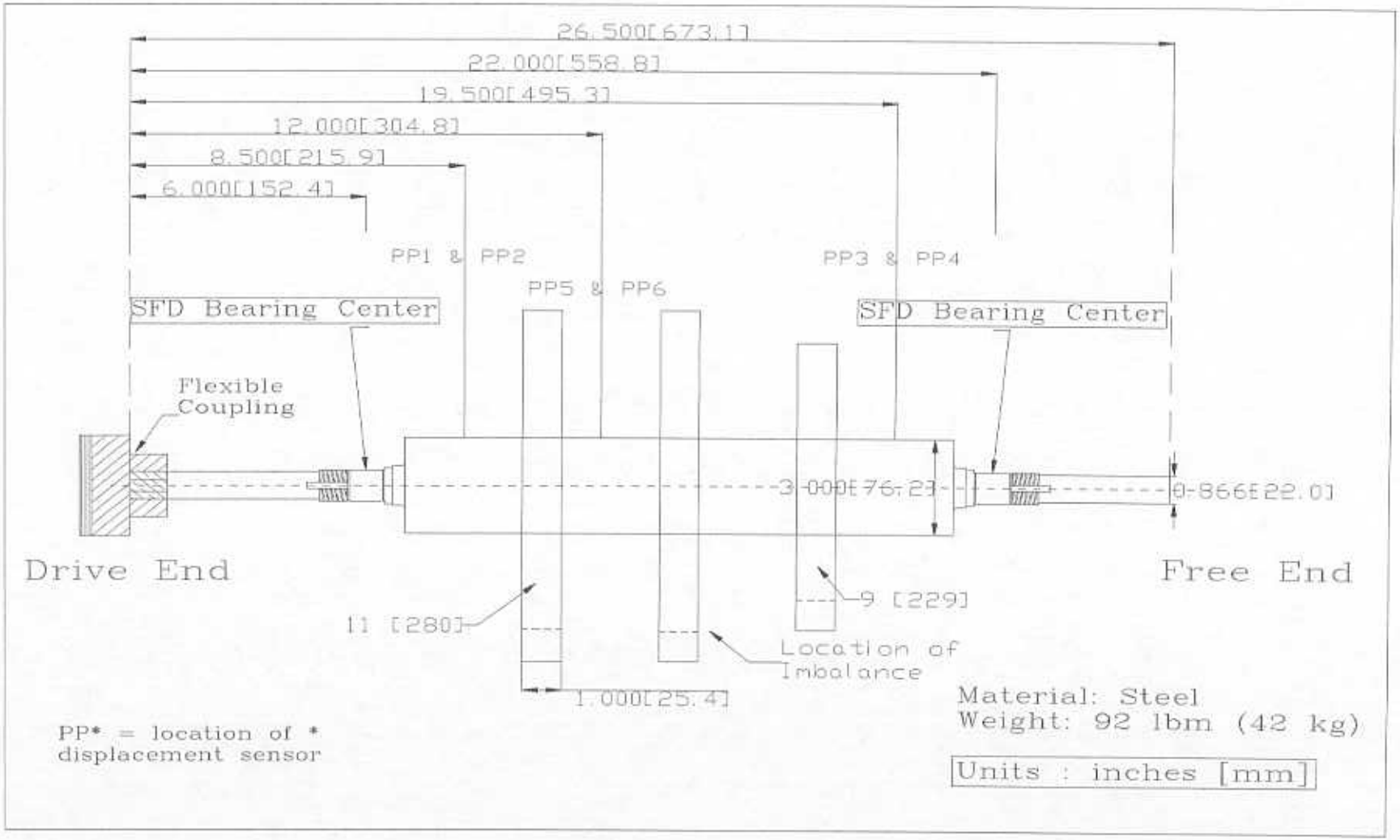

Figure 4. Test Rotor and Locations for Displacement Measurements

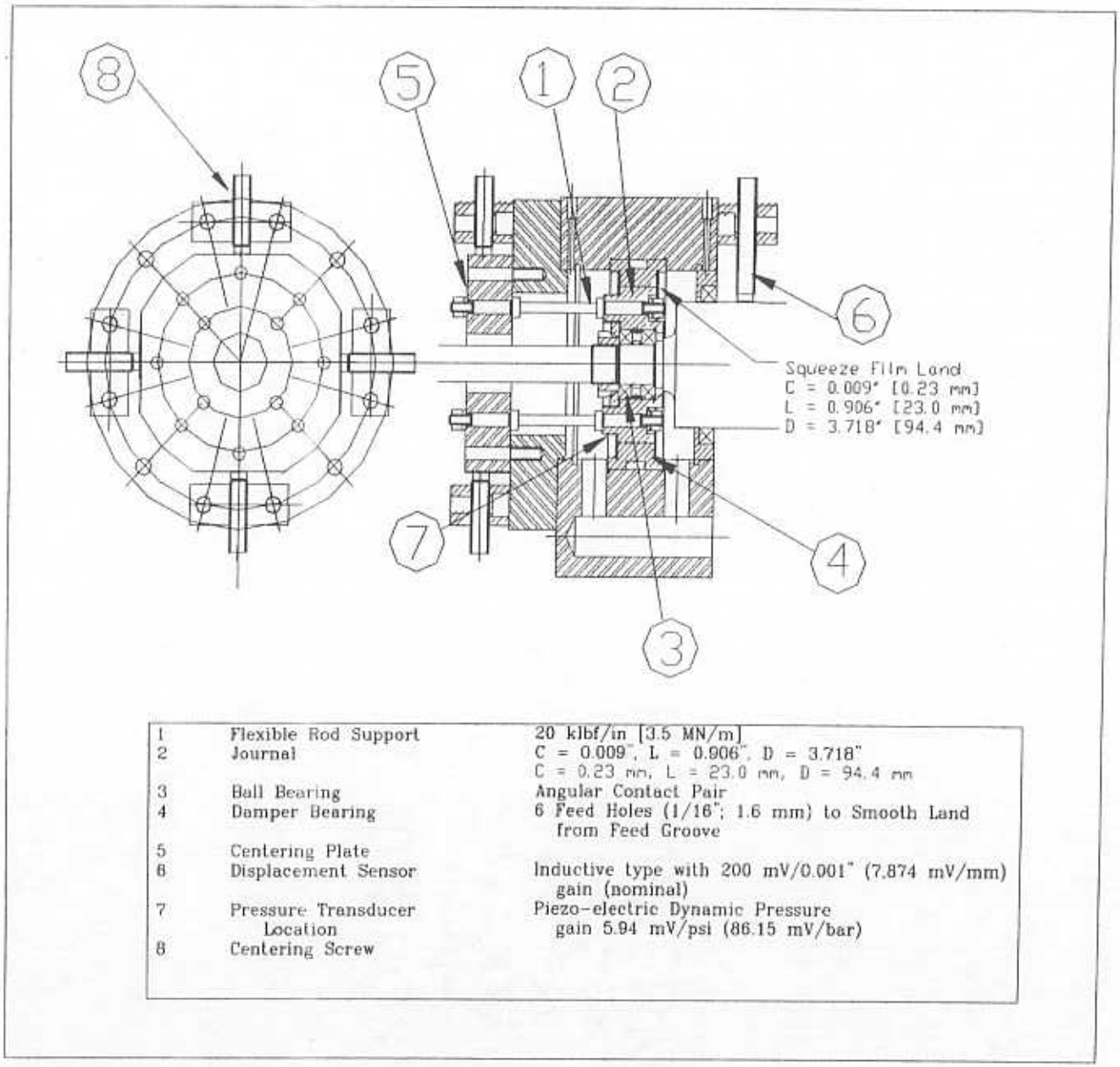

1	Flexible Rod Support	20 klbf/in [3.5 MN/m]
2	Journal	C = 0.009", L = 0.906", D = 3.718" C = 0.23 mm, L = 23.0 mm, D = 94.4 mm
3	Ball Bearing	Angular Contact Pair
4	Damper Bearing	6 Feed Holes (1/16"; 1.6 mm) to Smooth Land from Feed Groove
5	Centering Plate	
6	Displacement Sensor	Inductive type with 200 mV/0.001" (7.874 mV/mm) gain (nominal)
7	Pressure Transducer Location	Piezo-electric Dynamic Pressure gain 5.94 mV/psi (86.15 mV/bar)
8	Centering Screw	

Figure 5. Conventional Cylindrical Squeeze Film Damper and Flexible Support

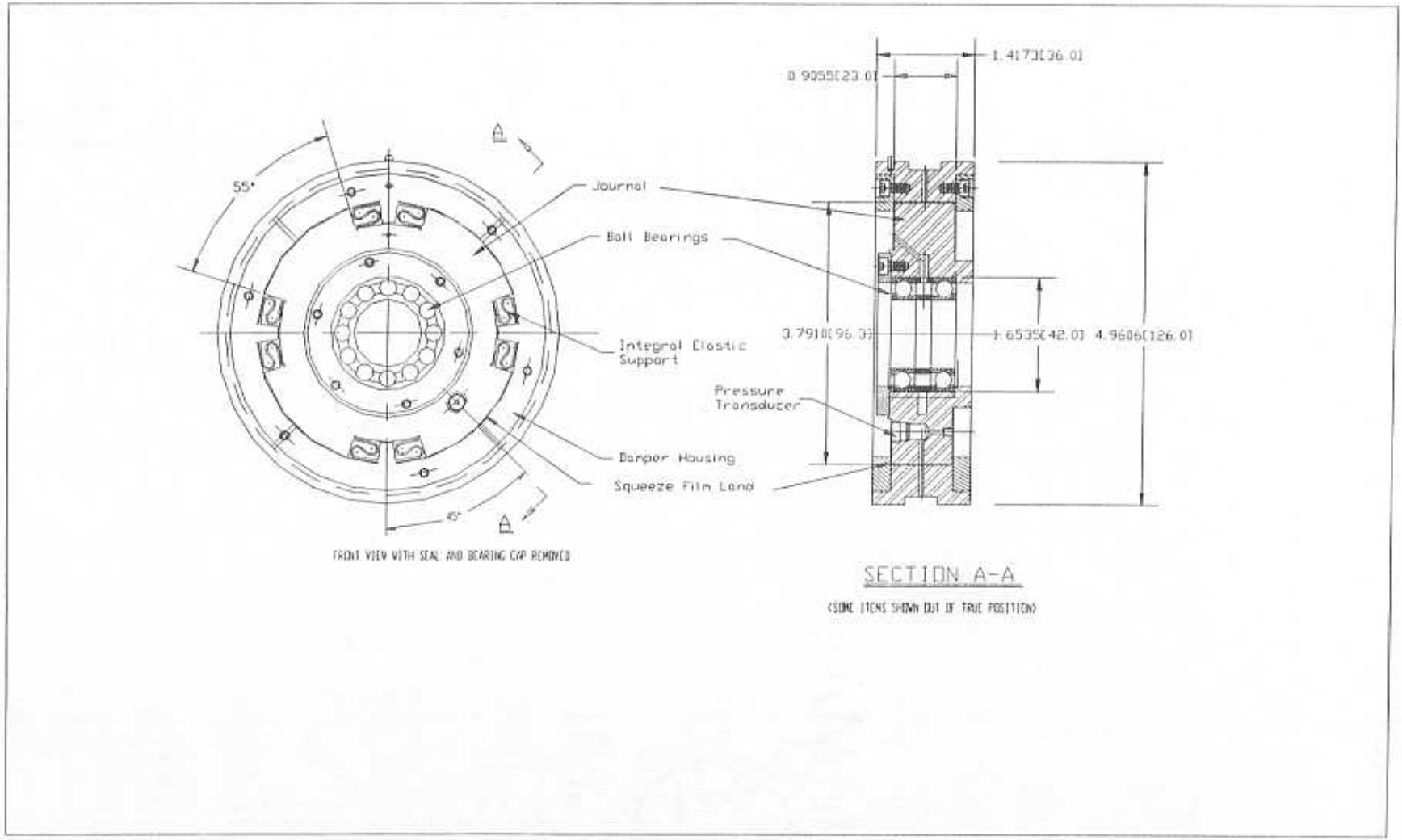

Figure 6. Integral KMC Squeeze Film Damper

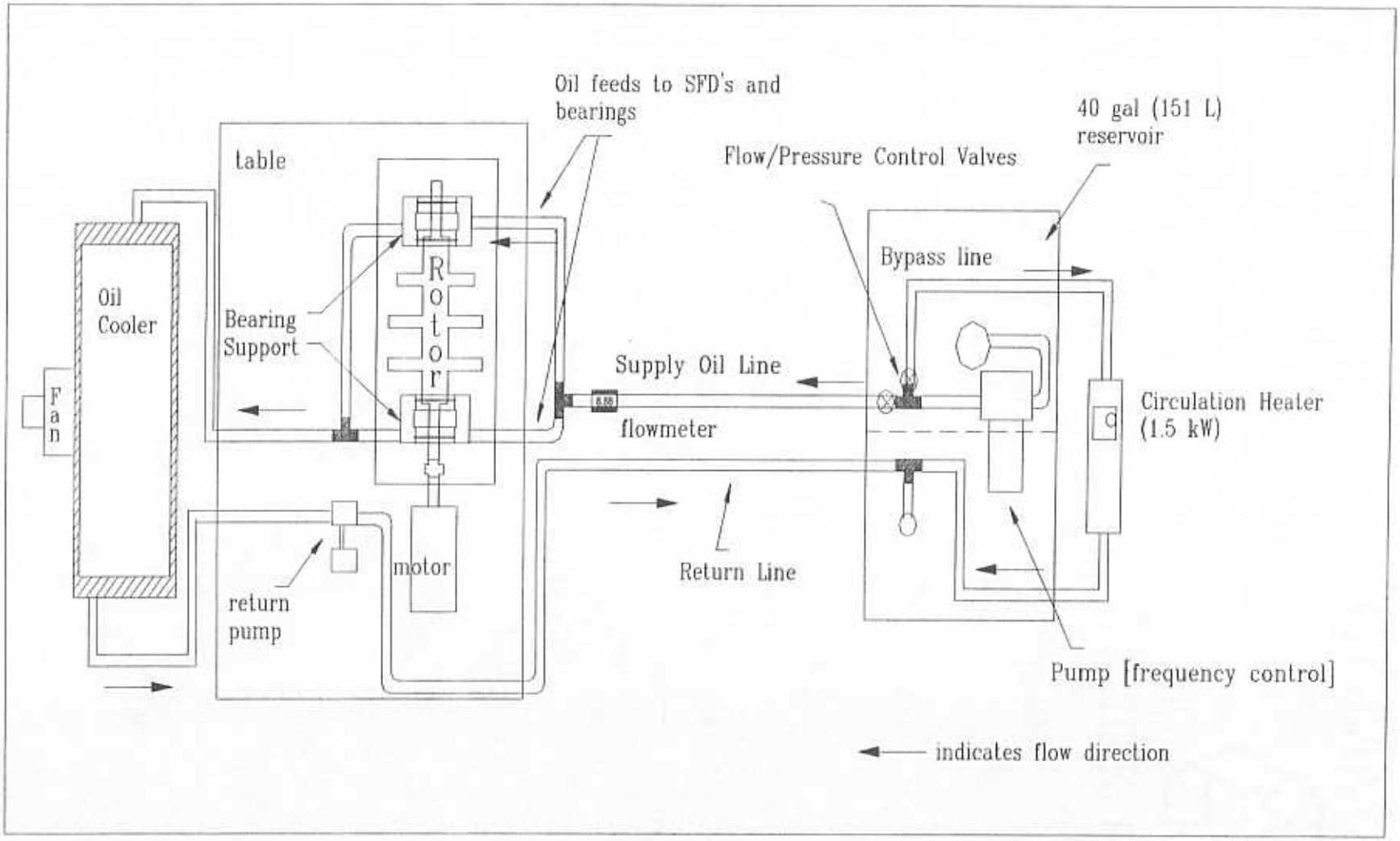

Figure 7. Lubrication System of Squeeze Film Damper Test Apparatus

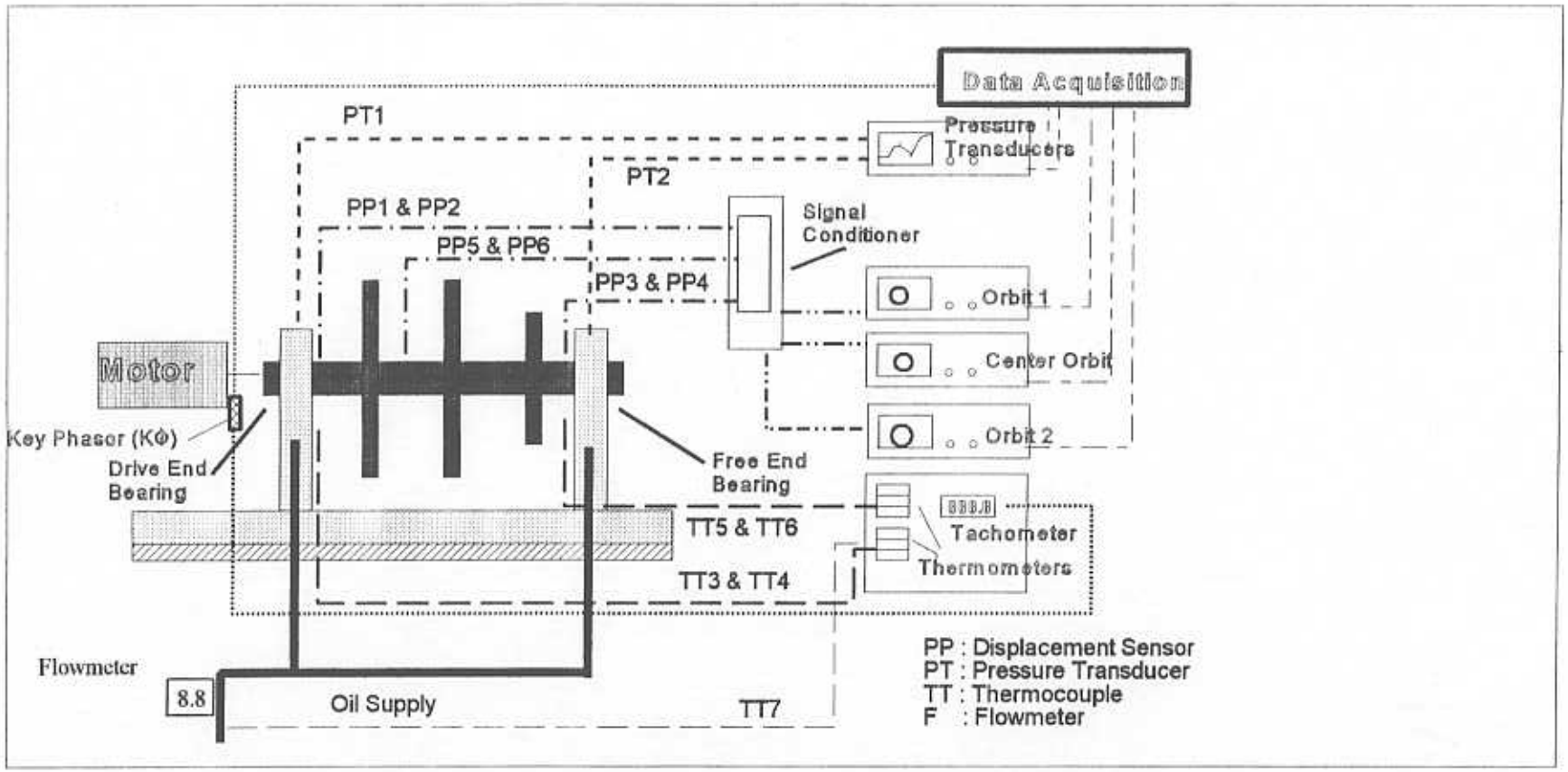

Figure 8. Instrumentation of Squeeze Film Damper Test Apparatus

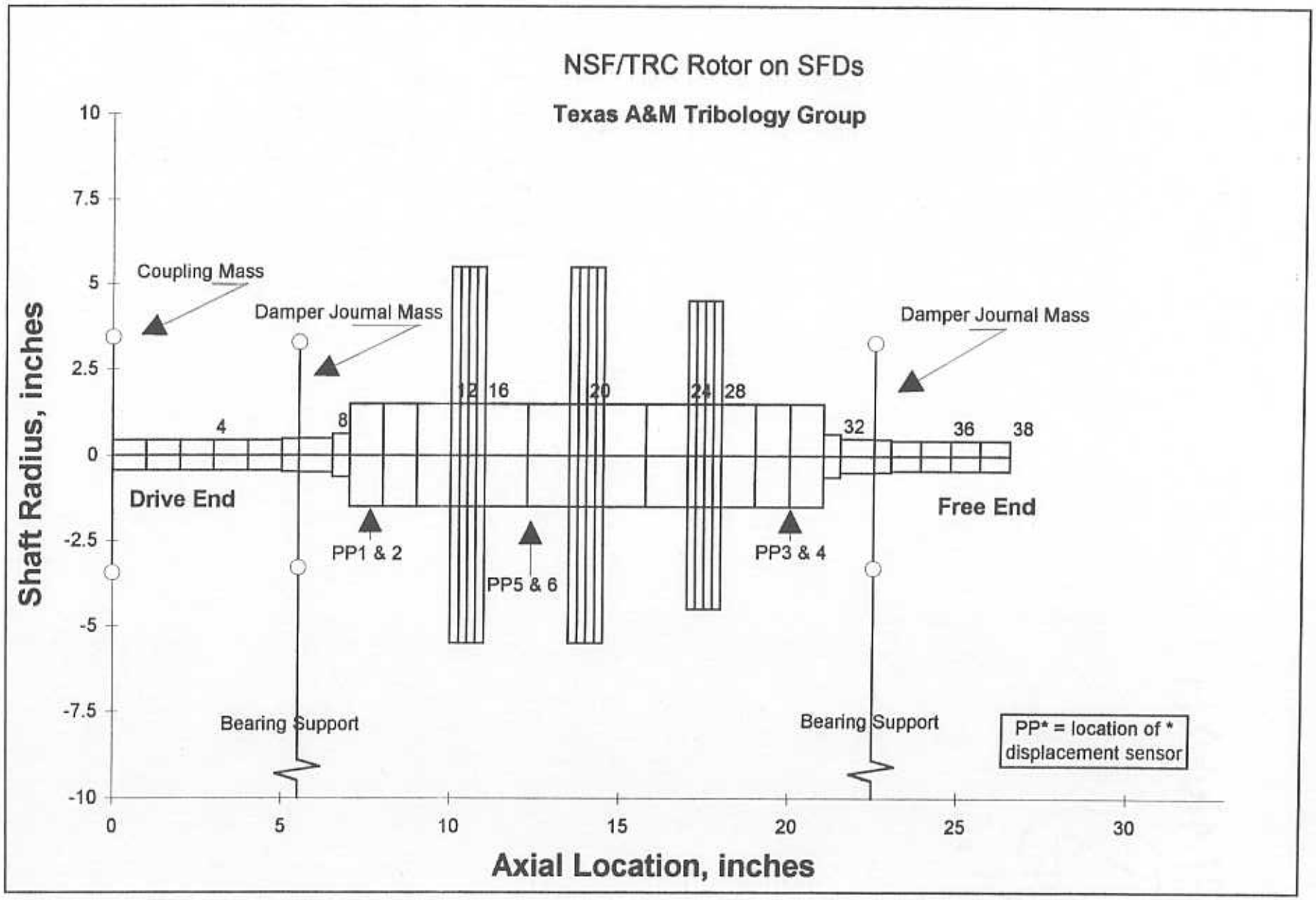

Figure 9. Structural Model of the Test Rotor

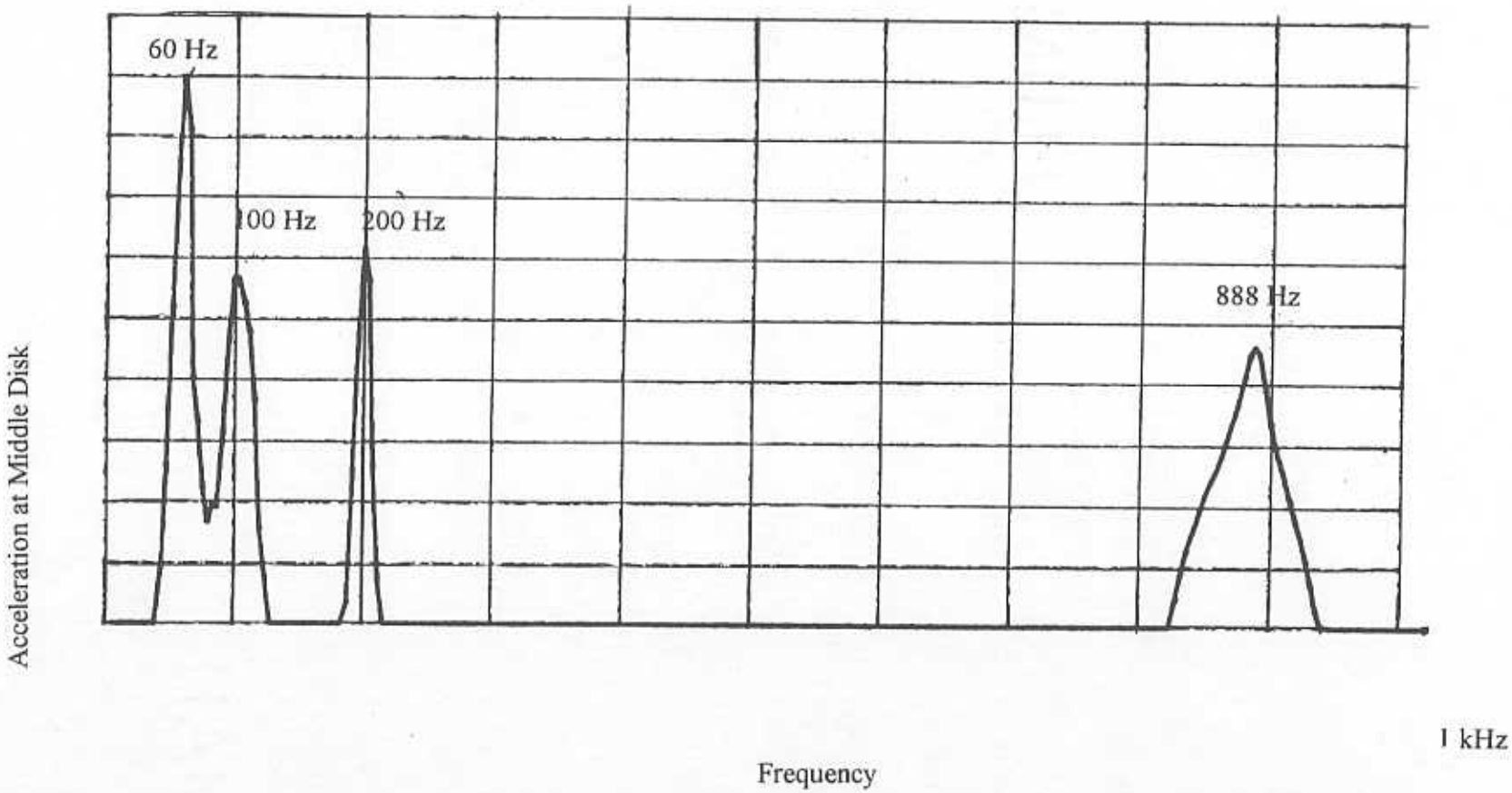

Figure 10. Frequency Spectrum of Free Vibration Response of Rotor at the Middle Disk When Rapped at Coupling in the Vertical Direction.

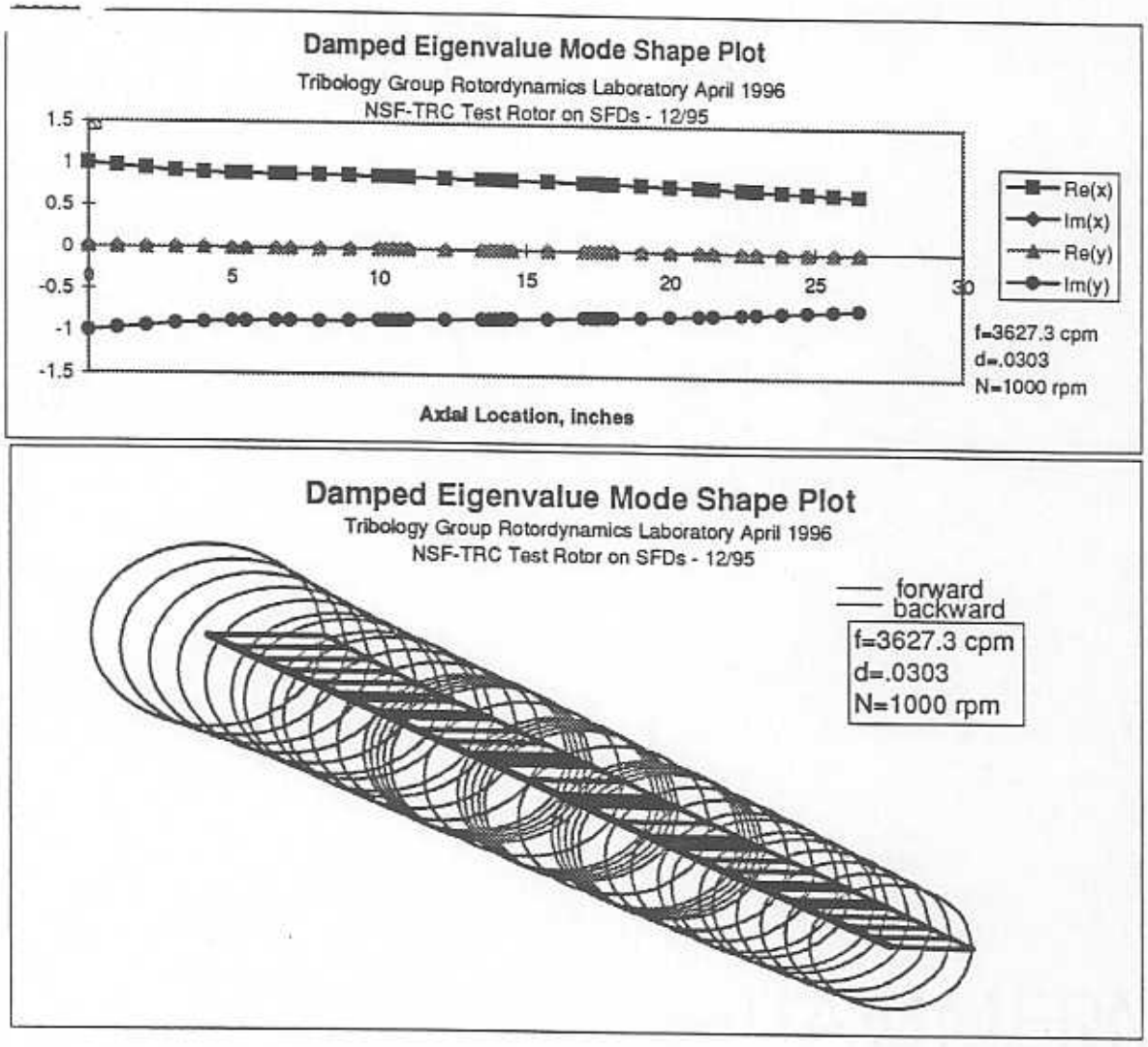

Figure 11a. First Mode Shape of Rotor on Squeeze Film Dampers

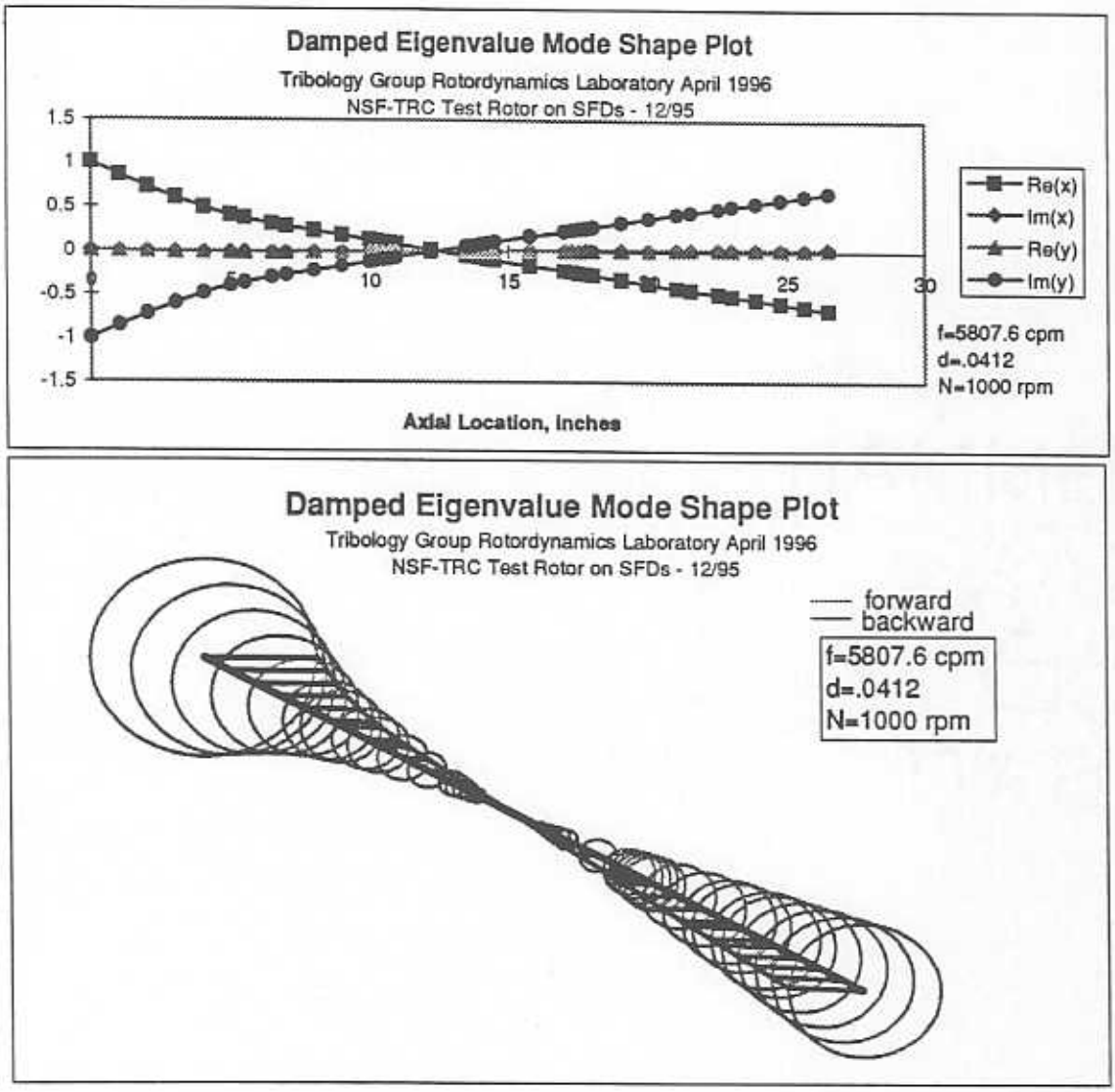

Figure 11b. Second Mode Shape of Rotor on Squeeze Film Dampers

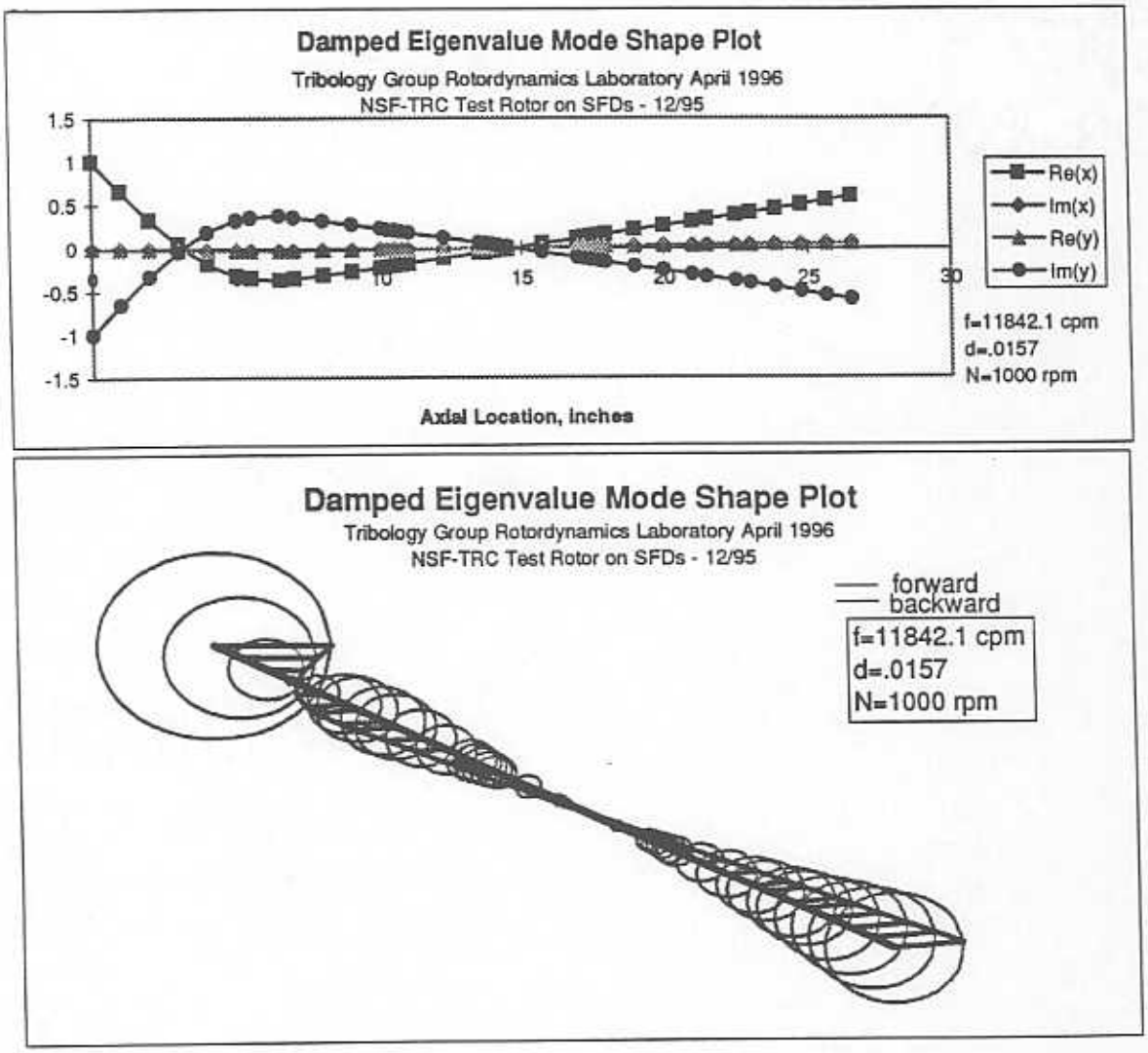

Figure 11c. Third Mode Shape of Rotor on Squeeze Film Dampers

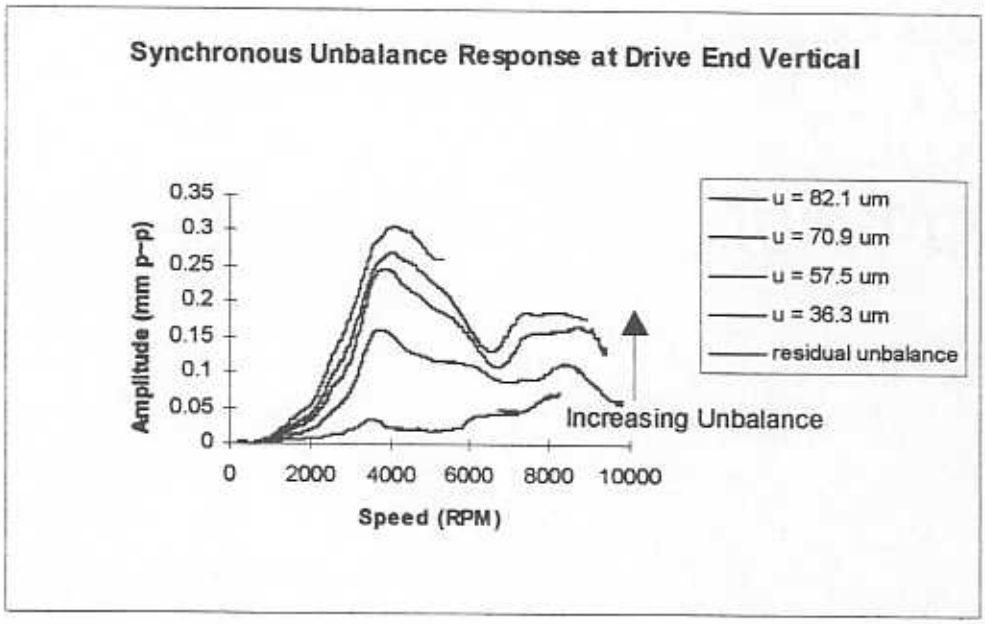

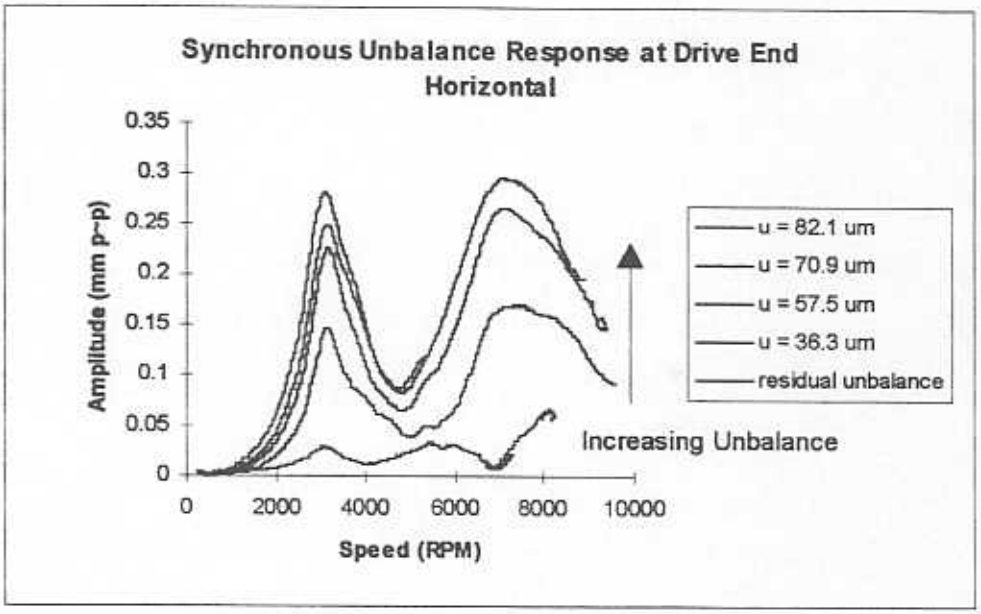

Figure 12. Synchronous Unbalance Response at Drive End [slow roll compensated]
a) Vertical, b) Horizontal

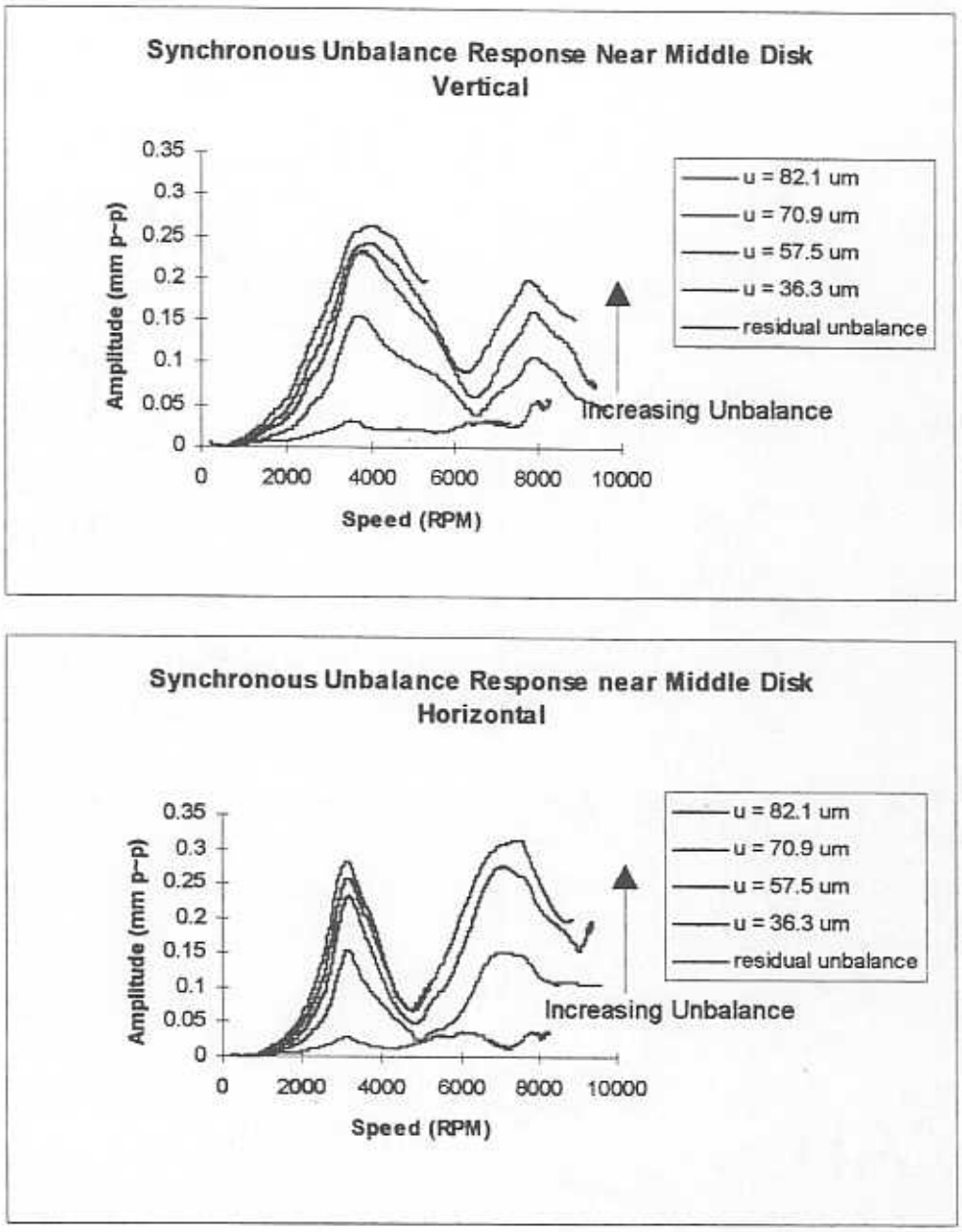

Figure 13. Synchronous Unbalance Response near Middle Disk [slow roll compensated]
a) Vertical, b) Horizontal

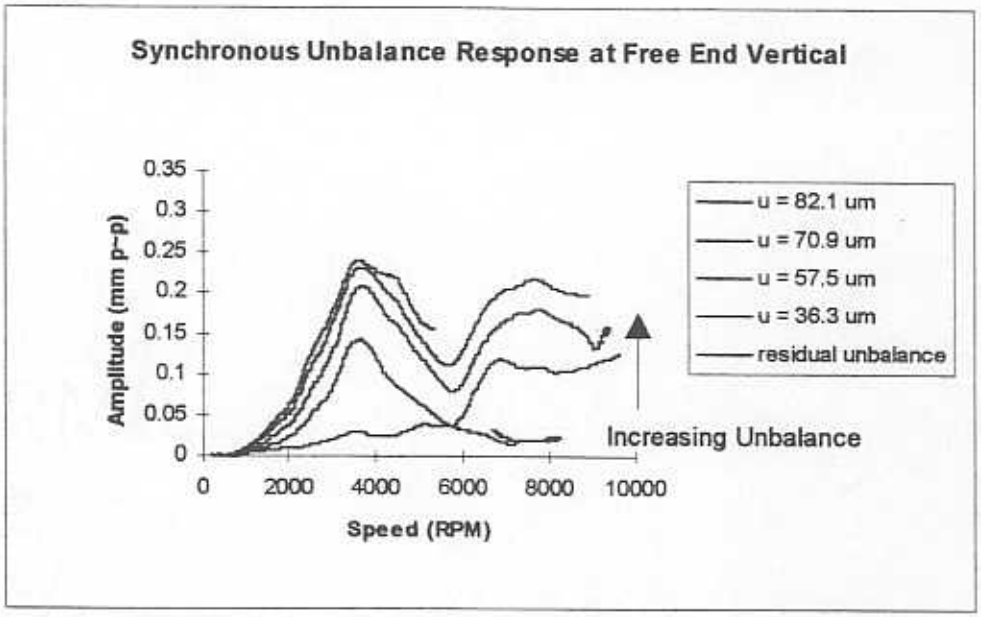

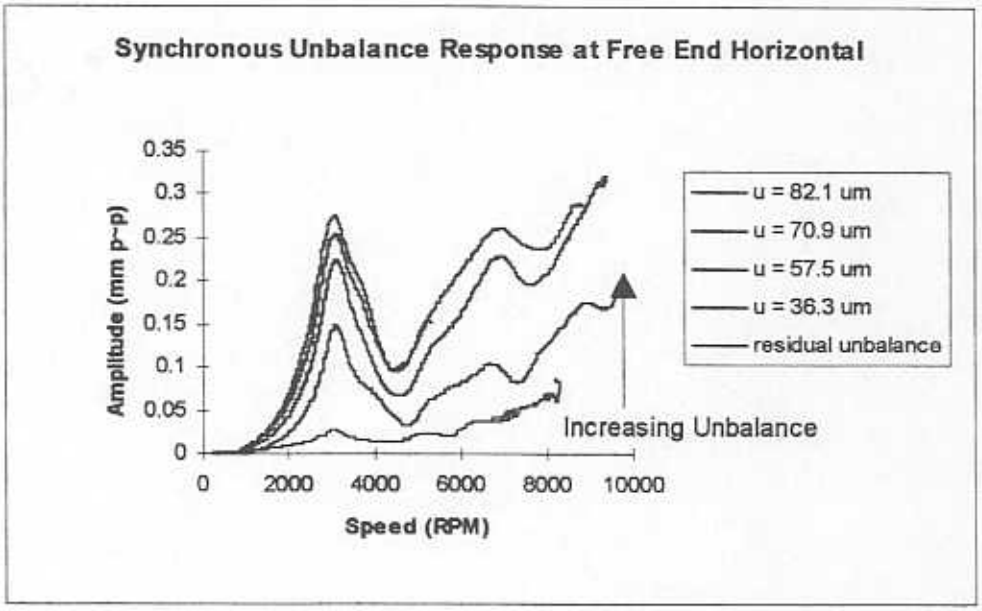

Figure 14. Synchronous Unbalance Response at Free End [slow roll compensated]
a) Vertical, b) Horizontal

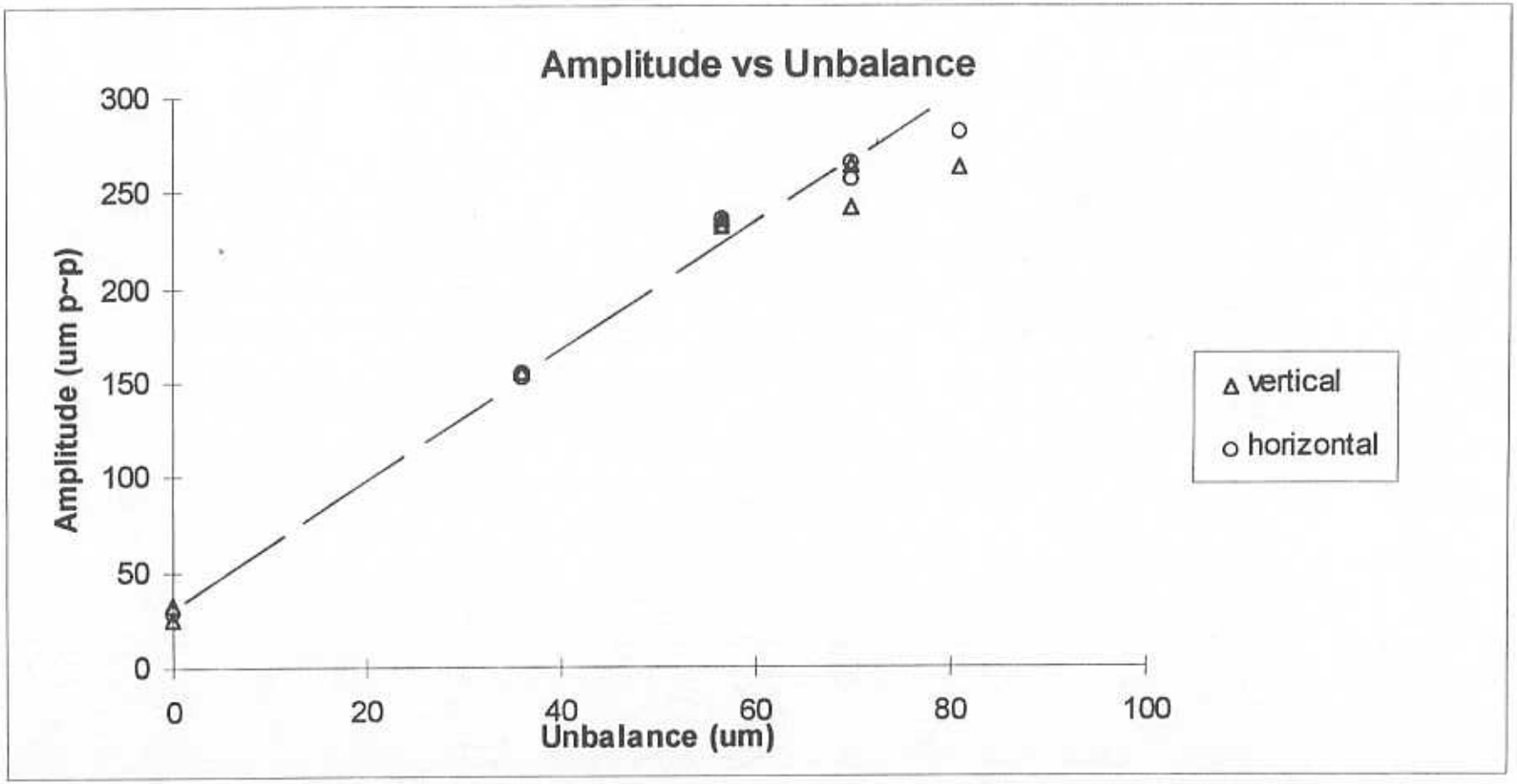

Figure 15. Peak Amplitude near Middle Disk Synchronous Unbalance Response vs Unbalance Magnitude at Middle Disk

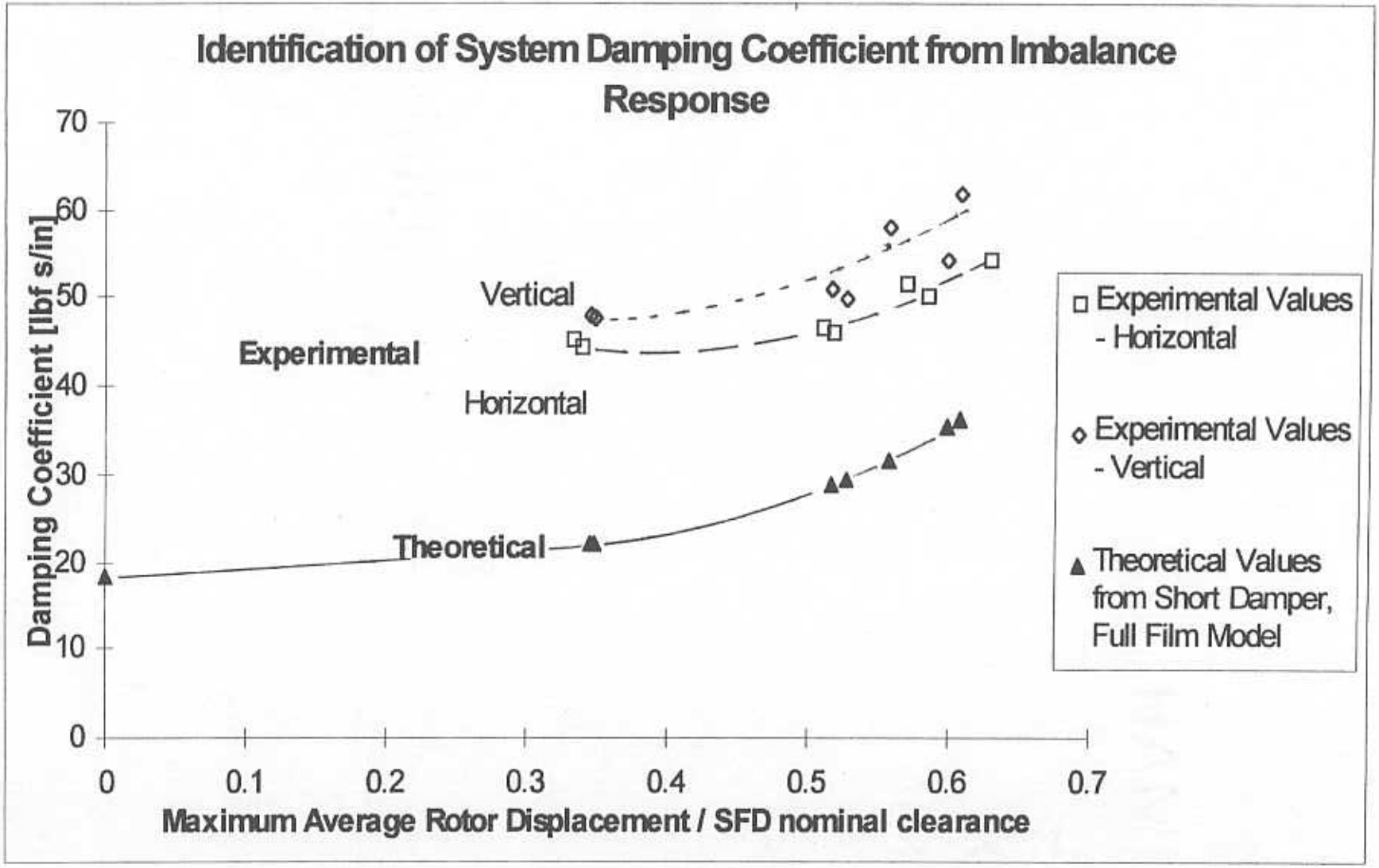

Figure 16. System Damping Coefficient from Imbalance Response (C_r = 222 µm (8.74 mils))

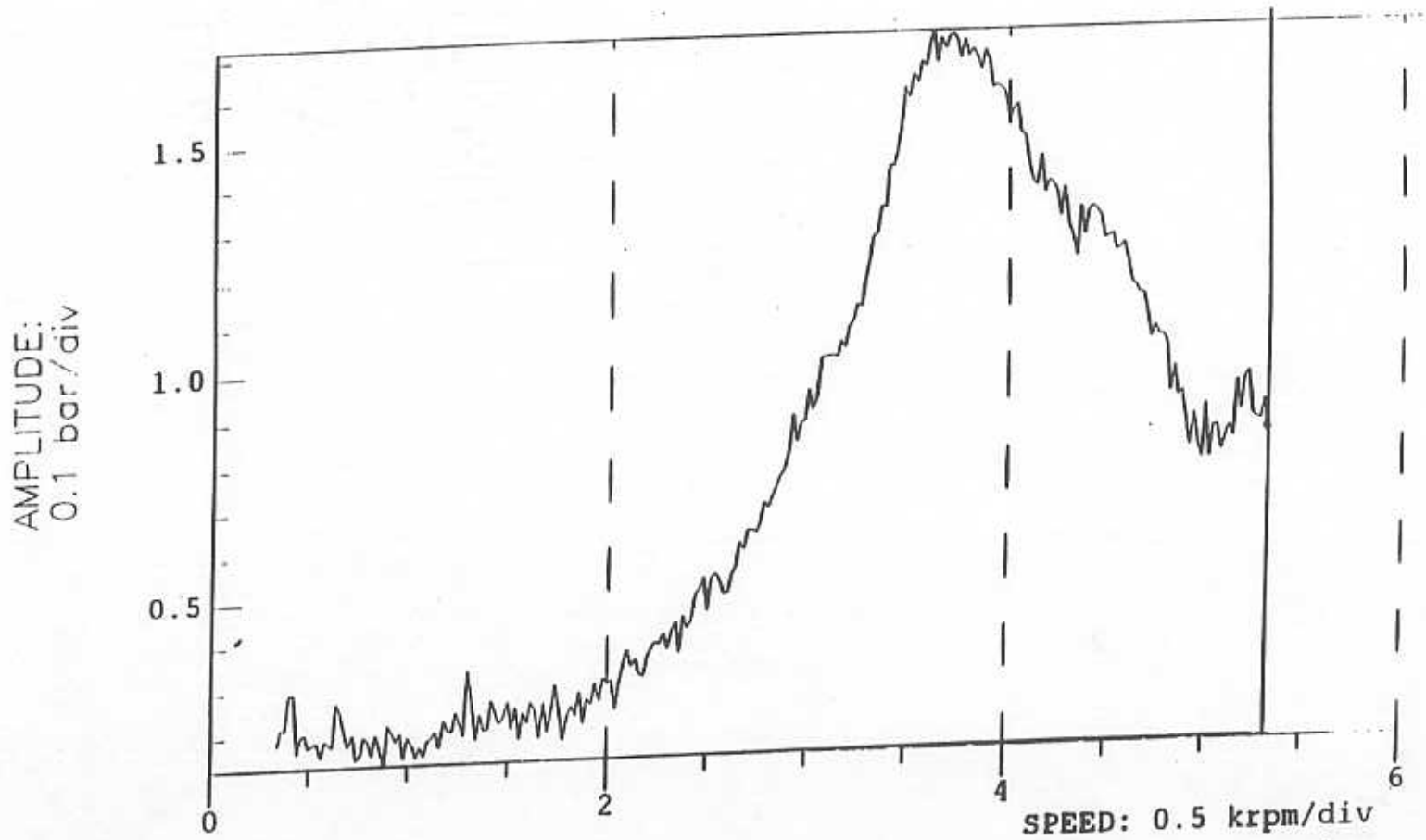

Figure 17. Peak to Peak Dynamic Pressures at Free End Squeeze Film Damper (vertical) with 80.7 µm Unbalance, ISO 10 oil at 91°F (μ = 12.5 cP).

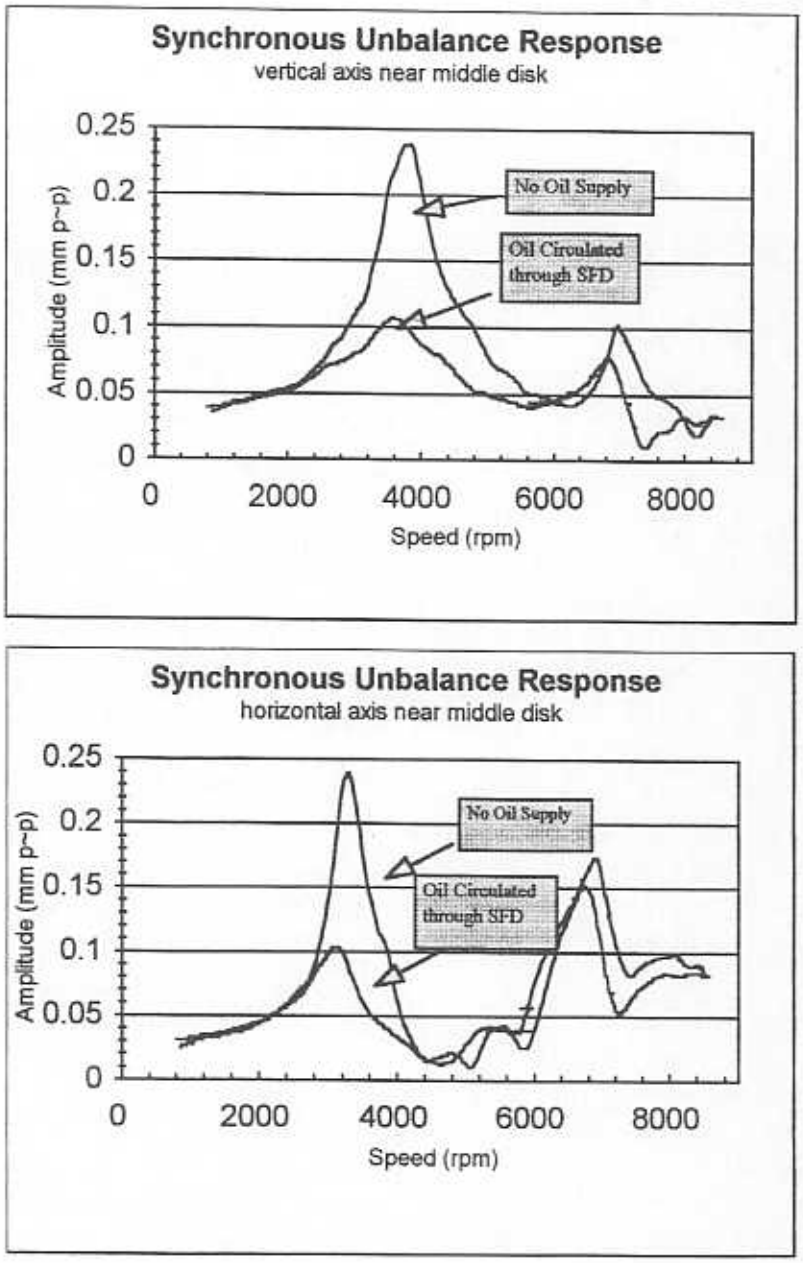

Figure 18. Run-up and Coast-down Test Measured near Middle Disk with Two Different Oil Supply Conditions: No Oil Supply, and Oil Circulated with a Feed Groove Pressure of 15 Psig. Lubricant Is Iso 10 Oil at 79°F (μ = 15.9 Cp). Unbalance = 28.3 μm at Small Disk.

a) Vertical Response

b) Horizontal Response

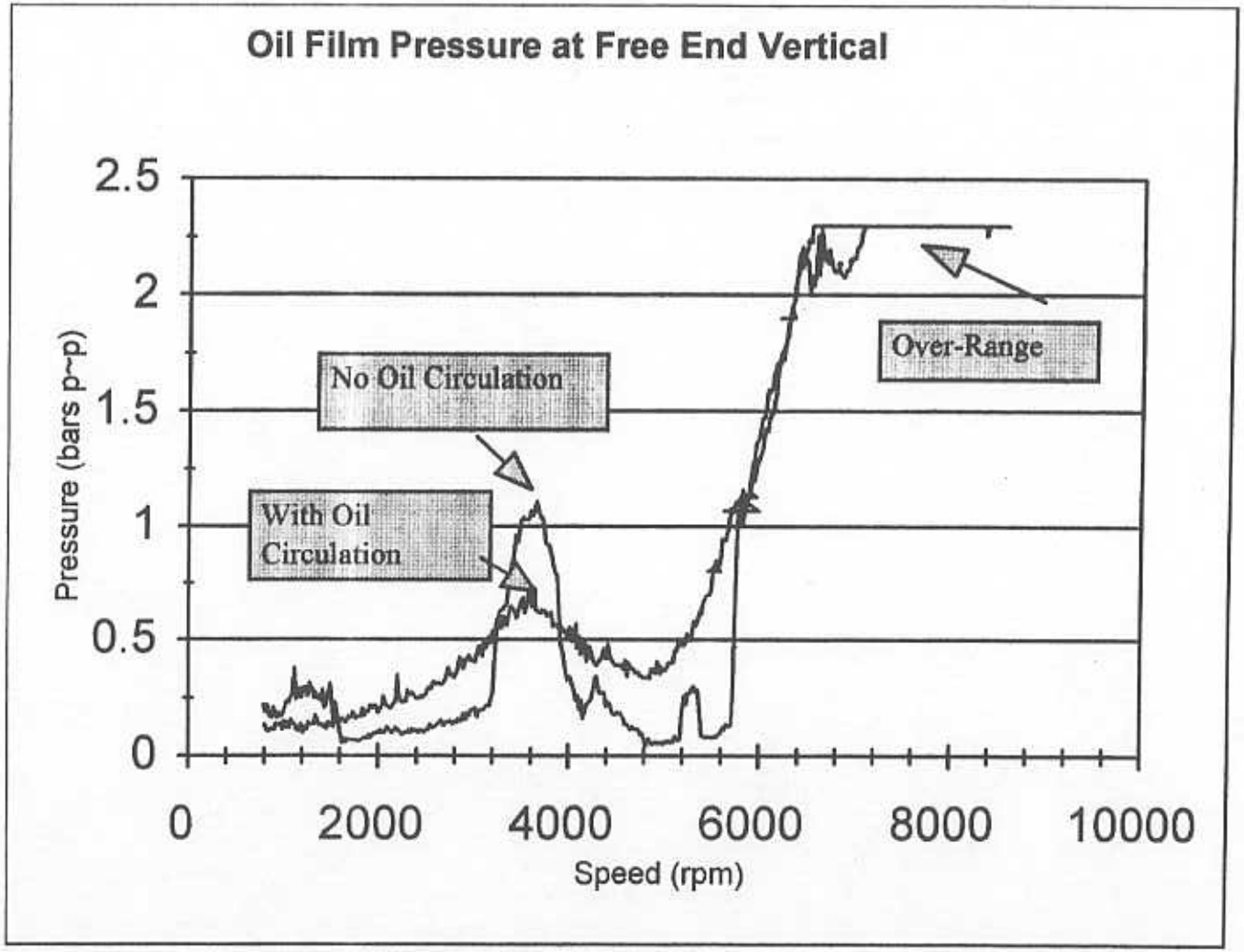

Figure 19. Oil Film Pressure in Free End (vertical) Squeeze Film Damper for Test Conditions in Figure 18.

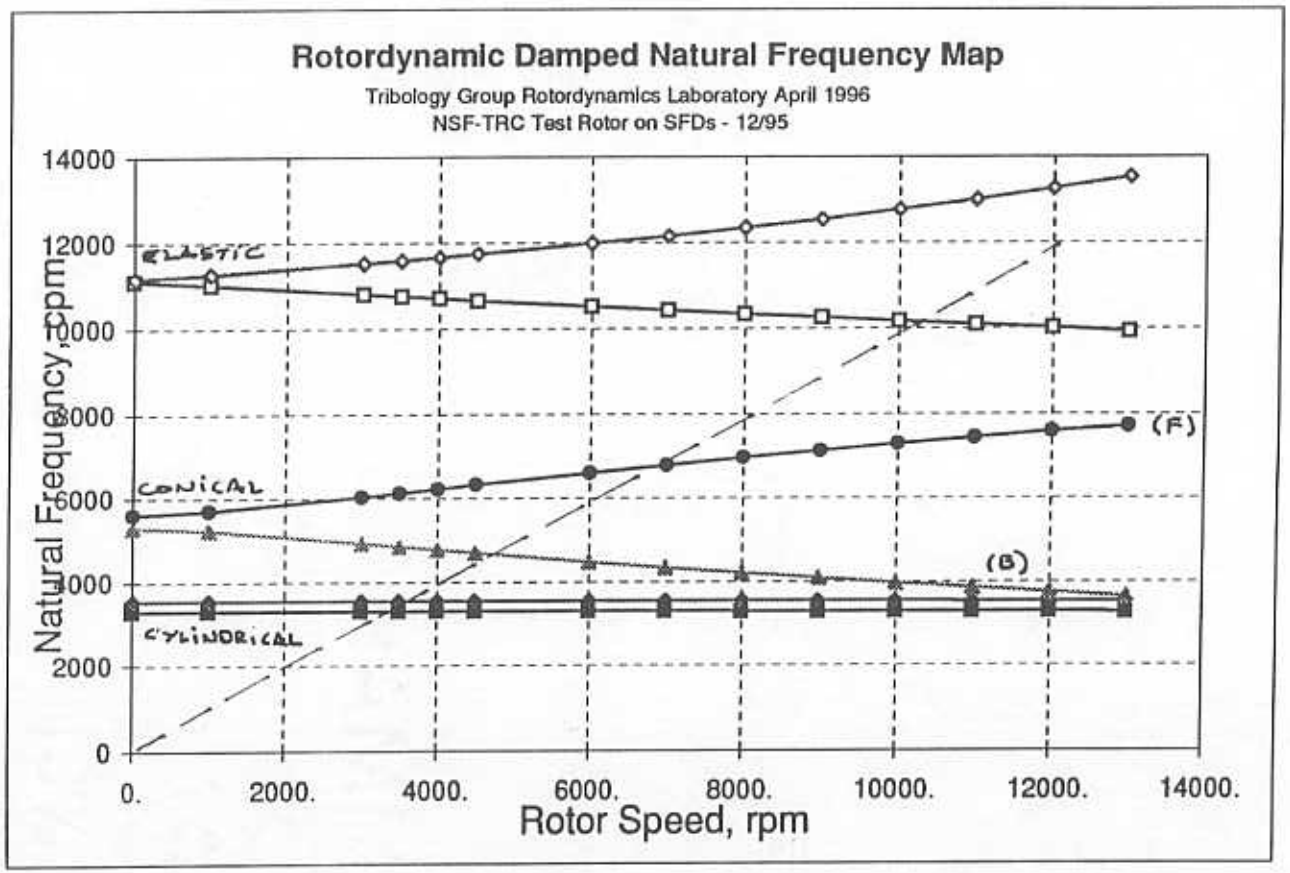

Figure 20. Predicted Natural Frequencies for Test Rotor. ($C_{xx} = C_{yy} = 23$ lbf s/in @ each bearing support)

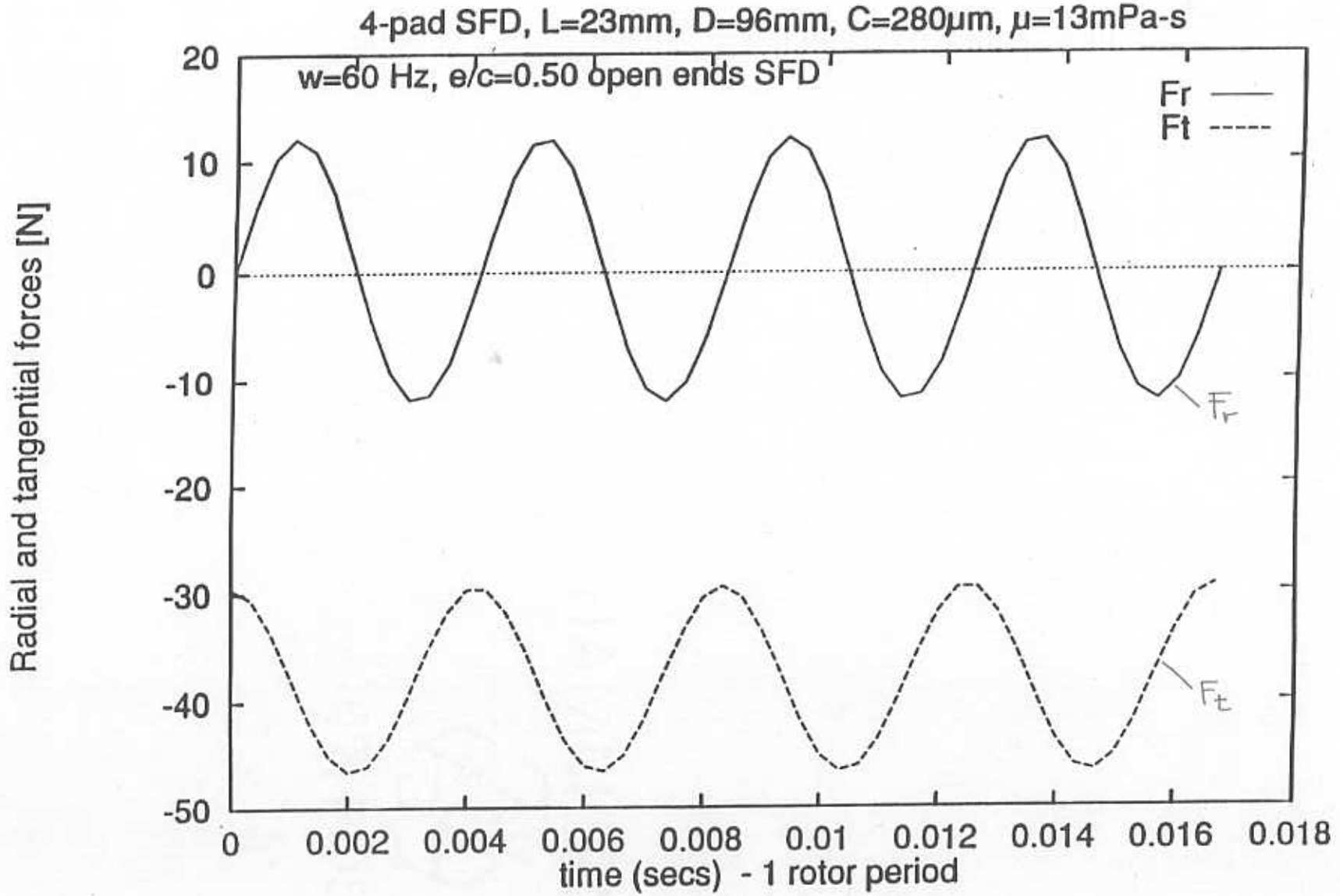

Figure 21. Forces from a 4-pad Integral Squeeze Film Damper

NSF/TRC SFD Project
Inventory

Base Plate
Battery for Current Boost
Bearing Supports
Bourdon type pressure gauges
Conventional SFD #2
Conventional SFD #1
Data Acquisition Software
Data Acquisition Hardware
Data Acquisition Computer
DC Motor (x2) [pumps]
DC Motor [drive]
Flexible Coupling
Foundation Table
Gear pumps (x2)
High Precision Ball Bearings (x4 pairs)
Integral SFD #2
Integral SFD #1
Motor Mount
Motor Faceplate [pump adaptor]
Oil - ISO 10
Oil Heater
Oil Cooler
Oil Reservoir
Optical Tachometer and Display
Power Supply [drive]
Power Supply (x2) [pump]
Proximity Probe Holder
Proximity Probes (x6)
Rotor
Safety Cover
Thermometers for K-Type thermocouples

Expenses for the NSF/TRC SFD Project

Date	Purchase	Supplier	Cost ($)
01-Jan-95	Oil Reservoir	Gatlin/Warren	$151.20
02-Feb-95	Printer Paper	Com ACC	$4.99
02-Feb-95	DC-Motor 15hp	ET Supply	$117.60
08-Feb-95	Ball Bearings	Motion Ind	$421.60
28-Mar-95	Machining conventional SFD	TMRF	$4,095.00
28-Mar-95	Machine Probe Stand & Motor Mount	ME Shop	$236.00
28-Mar-95	Machine Rotor and Housings	TMRF	$1,120.00
16-May-95	Steel Material for M.E. Shop	?	$232.00
18-May-95	Pump, Ball valves, Relief valve & Oil filte	Grainger	$170.57
19-May-95	Pump Motor & Supply	Cole-Parmer	$607.77
27-Jun-95	Pump/motor adaptors (2)	Grainger	$47.34
03-Jul-95	BNC Cables	Mid State Electronics	$270.60
13-Jul-95	Oil Cooler	Hydra Quip	$1,000.00
19-Jul-95	Coupling Body for Pump	Grainger	$3.81
24-Jul-95	Parker pumps (2)	Tex-a-Draulic	$137.30
26-Jul-95	Vibration Padding	Bryan Hose & Gasket	$30.66
01-Aug-95	Optical Sensor (Tachometer)	Cole Parmer	$264.18
02-Aug-95	Pressure Gauges (6)	Cole Parmer	$71.88
09-Aug-95	Hose & Fittings	BOTCO	$149.89
11-Aug-95	Nuts & Bolts	Ace Bolt and Screw	$10.46
14-Aug-95	Flowmeter / Thermocouple Wire	Cole Parmer	$352.03
14-Aug-95	Hose & Fittings	BOTCO	$120.19
15-Aug-95	Thermometers (5) & mounting plates	Omega	$0.00
16-Aug-95	Flexible Coupling/Oil seals (4)	Motion Ind.	$419.29
16-Aug-95	Hose & Fittings	BOTCO	$103.86
21-Aug-95	Oil Filters & Filter Head	Grainger	$27.42
05-Sep-95	SKF Bearings	Motion Ind.	$225.26
12-Sep-95	Lip Seals	Motion Ind.	$10.41
12-Sep-95	Fittings	BOTCO	$42.06
13-Sep-95	thermostat received (paid with cooler)	Hydraquip	$0.00
13-Sep-95	Roller Clutches	Bearing Inc	$66.49
14-Sep-95	Coupler and Plug	BOTCO	$31.62
21-Sep-95	fittings, hoses	BOTCO	$22.94
03-Oct-95	Valves, fittings	BOTCO	$25.06
05-Oct-95	Safety Carpet	Furrows	$54.04
17-Oct-95	Sockets and hose	BOTCO	$26.68
19-Oct-95	fittings and screws	BOTCO	$26.63
22-Oct-95	ratchet and socket	Sears	$31.98
26-Oct-95	tubing	Bryan Hose/Gskt	$16.80
02-Nov-95	relay	Grainger	$12.03
02-Nov-95	temp controller	Grainger	$71.53
02-Nov-95	bolts	Ace Bolt and Screw	$9.15
07-Nov-95	washers	Ace Bolt and Screw	$1.35
07-Nov-95	screws and braces	Furrow	$39.80
07-Nov-95	relay socket	Grainger	$3.11
17-Nov-95	screws and wood	Furrow	$29.39
17-Nov-95	jumper cables, wrench, mirror	Sears	$34.93
28-Nov-95	Battery	Sears	$86.99
28-Nov-95	Blower....reimbursement for Dan	Wal-Mart	$32.41
07-Dec-95	welding cable	Bob Smith	$58.80

11-Dec-95	cable fittings	Dealers Elec.	$13.90
05-Jan-96	Bolts	Ace Bolt & Screw	$2.51
05-Jan-96	Paper	Com. Acc.	$9.90
17-Jan-96	Fittings, power strips	BOTCO	$27.94
17-Jan-96	AC splitter	Furrow	$7.60
17-Jan-96	BNC cables and connectors	Mid State Elec	$76.58
22-Jan-96	Welding Cable for DC motor	Bob Smith	$42.00
23-Jan-96	Cable Ends	Dealers Electric	$15.24
24-Jan-96	Battery Switch	Hi/Lo	$18.29
24-Jan-96	BNC cables	Mid State Electronics	$50.00
24-Jan-96	Needle Valve	BOTCO	$23.34
05-Feb-96	Relay, relay socket, heater	Grainger	$182.54
05-Feb-96	Switch	Grainger	$11.85
08-Feb-96	Hoses and fittings	BOTCO	$123.22
08-Feb-96	Relay and socket	Grainger	$16.36
09-Feb-96	Gear Pump	Tex-a-Draulic	$147.11
09-Feb-96	Pump coupling and pump face	Grainger	$27.27
09-Feb-96	Pump Controller and DC motor	Cole Parmer	$587.54
14-Feb-96	Zip Drive	Circuit City	$199.97
20-Feb-96	Fittings	BOTCO	$11.97
14-Apr-96	ADRE software and DAIU (8 channels)	Bently Nevada	$12,082.00
14-Apr-96	Pentium 120 PC for ADRE/DAIU	Micro Age	$2,905.00
17-Apr-96	Pressure Gauges (3)	Cole Parmer	$71.05
		TOTAL	**$27,778.28**